WY-18/01F

FINAL REPORT

State of Wyoming
Department of Transportation

Performance Evaluation of Rigid Snow Supporting Structures at the Milepost 151 Avalanche, Jackson, Wyoming

By:
InterAlpine Engineers, LLC
24 W. Quartz Rd.
Flagstaff, AZ 86005
September 2017

Notice

This document is disseminated under the sponsorship of the Wyoming Department of Transportation (WYDOT) in the interest of information exchange. WYDOT assumes no liability for the use of the information contained in this document.

WYDOT does not endorse products or manufacturers. Trademarks or manufacturers' names appear in this report only because they are considered essential to the objective of the document.

Quality Assurance Statement

WYDOT provides high-quality information to serve Government, industry, and the public in a manner that promotes public understanding. Standards and policies are used to ensure and maximize the quality, objectivity, utility, and integrity of its information. WYDOT periodically reviews quality issues and adjusts its programs and processes to ensure continuous quality improvement.

Further, if the report contains either confidential information or, if any information in the report is subject to copyright, patent, or trademark requirements, the report must contain additional disclaimers that may be obtained through the Research Center.

Creative Commons

TECHNICAL REPORT DOCUMENTATION PAGE

1. Report No. WY-18/01F	**2. Government Accession No.**	**3. Recipient's Catalog No.**
4. Title and Subtitle Performance Evaluation of Rigid Snow Supporting Structures at the Milepost 151 Avalanche, Jackson, Wyoming		**5. Report Date** September 2017 **6. Performing Organization Code:**
7. Author(s) Joshua Hewes (0000-0002-2098-4399)		**8. Performing Organization Report No.** RS07-212
9. Performing Organization Name and Address InterAlpine Engineers, LLC 24 W. Quartz Rd. Flagstaff, AZ 86005		**10. Work Unit No.** **11. Contract or Grant No.** RS07-212
12. Sponsoring Agency Name and Address Wyoming Department of Transportation 5300 Bishop Blvd Cheyenne, WY 82009-3340 WYDOT Research Center (307)777-4182		**13. Type of Report and Period** Final Report – December 28, 2012 to September 30, 2017 **14. Sponsoring Agency Code** WYDOT
15. Supplementary Notes		

16. Abstract

In order to validate the methods used to design a novel, rigid snow supporting structure system, a research project to experimentally monitor for two winter seasons and visually inspect it over three summers was performed for WYDOT through their Research Center. One snow supporting structure was instrumented with pressure transducers to record down-slope snow pressures imparted to the supporting surface. Snow depth immediately uphill of the structure was measured as was ambient and snowpack temperature. Additionally, strain gages mounted to parts of the structure were used to back-check the recorded snow forces by static equilibrium. Pressure distributions with depth were parabolic and maximum at approximately mid-height of the structure. Average, uniform snow pressures determined from the experimental data were compared to pressures predicted by the Swiss Guide and McClung's analytical models. Maximum uniform pressures over the two winter seasons were 38 percent and 22 percent greater than the Swiss Guide and McClung snow pressure predictions. Variation of snow pressure across the lateral dimension (width) of the structure was also investigated and the maximum experimental end-effect factor of 4.9 correlated very well with the end-effect factor specified in the Swiss Guide of 4.75. The location of snow force resultants were also calculated for all data and an average value of 56 percent of the snowpack height measured from the ground surface was obtained. This compared well with the assumed 50 percent or mid-height location prescribed by the Swiss Guide. Finally, maximum local pressures across the height of the structure were compared to the experimental uniform pressures and an average ratio of maximum-to-average of 1.8 was obtained. This is greater than the Swiss Guide's assumption of 1.3, and it is recommended that individual members such as crossbeams be designed using the Swiss Guide average pressure increased by the 1.8 factor. In general, it was shown that the assumptions and design values produced using the Swiss Guide expressions can be used for an irregular plan layout of snow supporting structures such as that used at the Milepost 151 Avalanche.

17. Key Words Avalanche Defense, Snow Pressure, Snow Supporting Structure, Wyoming,	**18. Distribution Statement** This document is available through the National Transportation Library and the Wyoming State Library.

19. Security Classif. (of this report) Unclassified	**20. Security Classif. (of this page)** Unclassified	**21. No. of Pages** 81	**22. Price**

Form DOT F 1700.7 (8-72) Reproduction of completed page authorized.

SI* (MODERN METRIC) CONVERSION FACTORS

APPROXIMATE CONVERSIONS TO SI UNITS

Symbol	When You Know	Multiply By	To Find	Symbol
		LENGTH		
in	inches	25.4	millimeters	mm
ft	feet	0.305	meters	m
yd	yards	0.914	meters	m
mi	miles	1.61	kilometers	km
		AREA		
in^2	square inches	645.2	square millimeters	mm^2
ft^2	square feet	0.093	square meters	m^2
yd^2	square yard	0.836	square meters	m^2
ac	acres	0.405	hectares	ha
mi^2	square miles	2.59	square kilometers	km^2
		VOLUME		
fl oz	fluid ounces	29.57	milliliters	mL
gal	gallons	3.785	liters	L
ft^3	cubic feet	0.028	cubic meters	m^3
yd^3	cubic yards	0.765	cubic meters	m^3
		NOTE: volumes greater than 1000 L shall be shown in m^3		
		MASS		
oz	ounces	28.35	grams	g
lb	pounds	0.454	kilograms	kg
T	short tons (2000 lb)	0.907	megagrams (or "metric ton")	Mg (or "t")
		TEMPERATURE (exact degrees)		
^oF	Fahrenheit	5 (F-32)/9 or (F-32)/1.8	Celsius	^oC
		ILLUMINATION		
fc	foot-candles	10.76	lux	lx
fl	foot-Lamberts	3.426	$candela/m^2$	cd/m^2
		FORCE and PRESSURE or STRESS		
lbf	poundforce	4.45	newtons	N
lbf/in^2	poundforce per square inch	6.89	kilopascals	kPa

APPROXIMATE CONVERSIONS FROM SI UNITS

Symbol	When You Know	Multiply By	To Find	Symbol
		LENGTH		
mm	millimeters	0.039	inches	in
m	meters	3.28	feet	ft
m	meters	1.09	yards	yd
km	kilometers	0.621	miles	mi
		AREA		
mm^2	square millimeters	0.0016	square inches	in^2
m^2	square meters	10.764	square feet	ft^2
m^2	square meters	1.195	square yards	yd^2
ha	hectares	2.47	acres	ac
km^2	square kilometers	0.386	square miles	mi^2
		VOLUME		
mL	milliliters	0.034	fluid ounces	fl oz
L	liters	0.264	gallons	gal
m^3	cubic meters	35.314	cubic feet	ft^3
m^3	cubic meters	1.307	cubic yards	yd^3
		MASS		
g	grams	0.035	ounces	oz
kg	kilograms	2.202	pounds	lb
Mg (or "t")	megagrams (or "metric ton")	1.103	short tons (2000 lb)	T
		TEMPERATURE (exact degrees)		
^oC	Celsius	1.8C+32	Fahrenheit	^oF
		ILLUMINATION		
lx	lux	0.0929	foot-candles	fc
cd/m^2	$candela/m^2$	0.2919	foot-Lamberts	fl
		FORCE and PRESSURE or STRESS		
N	newtons	0.225	poundforce	lbf
kPa	kilopascals	0.145	poundforce per square inch	lbf/in^2

TABLE OF CONTENTS

LIST OF FIGURES

LIST OF TABLES

CHAPTER 1: INTRODUCTION

1.1 Background

The Milepost 151 Avalanche is located within the Teton National Forest and sits above US 89/191 at mile marker 151 on a west-facing slope approximately 1.5 miles south of the town of Jackson, WY. US 89/191 has four lanes and carries an estimated 8,000 vehicles per day in the winter months. The 151 Avalanche is a well-known hazard and avalanches have struck vehicles in the past, resulting in crashes, traffic delays, and the need for debris clean-up by WYDOT maintenance crews. The site has, historically, avalanched onto the road 1 to 2 times per year on average before the design and installation of 87 steel snow supporting structures (SSS) in 2012.

Prior to the Milepost 151 SSS project, the use of SSS in the starting zone to mitigate avalanche risk along a major roadway was without precedent in the United States, despite a long and successful history of their use for the same purpose throughout Europe. SSS in Europe are typically deployed in a very linear, orderly fashion because this is the most efficient arrangement. The layout of SSS at the Milepost 151 however, is much more "organic" in appearance, blending in with the surroundings, and with individual SSS arranged as either single, double, triple, or quadruple groupings of individual SSS (figure 1). SSS groups are offset in the fall line – not positioned in rows along the same contour line. This configuration was selected in order to meet National Environmental Policy Act (NEPA) requirements for the project for visual retention (minimal disruption of the existing landscape). Because no domestic design standards were available to guide the design of SSS for the Milepost 151, the Swiss technical standard "Defense Structures in Avalanche Starting Zones, Technical Guideline as an Aid to Enforcement" (referred to herein as the "Swiss Guide") was used as the basis for design of the facility (FOEN 2006). While use the of Swiss Guide was considered best practices at the time of the project, the significant difference in deployment technique and the fact that the standard was developed overseas suggests verification is appropriate as a matter of due diligence.

Figure 1 Organic deployment of SSS at the Milepost 151 site

1.2 Problem Statement

The Wyoming Department of Transportation (WYDOT) has recently begun efforts to reduce the usage of artillery and hand-deployed explosives for avalanche control work along State maintained roads and highways. New and different technologies that either reduce or eliminate altogether the need for maintenance worker attention during periods of high avalanche danger have been implemented by WYDOT. Many of these novel approaches to avalanche risk mitigation were developed first in Europe, and then imported into domestic practice in large part due to WYDOT's research efforts. In 2005, the WYDOT Research Center funded a project to assess the feasibility of using constructed, passive avalanche defense in the form of steel SSS in the starting zone of the Milepost 151 Avalanche. Results of that research led directly to the development of a project in 2011 to design and construct a series of snow supporting structures at the Milepost 151 site.

Because the Milepost 151 SSS project was the first U.S. domestic project to utilize SSS in a more random deployment scheme, and since no design standards or previous practical experience were available to the project design engineers, a research project focused on the monitoring of the facility was proposed to the WYDOT Research Center in 2012.

1.3 Study Objectives

This research study intended to accomplish the following project objectives:

- Measure experimentally the spatial and temporal distribution of snow pressure acting on a snow supporting structure sited in the starting zone of the Milepost 151 Avalanche.
- Compare the experimental snow pressures with those predicted by the Swiss Guide.
- Monitor the on-going performance and "health" of the entire array of 87 SSS at the Milepost 151 site by annual visual inspections.
- Provide the requisite fundamental understanding and background information to be used in the development of a U.S. design guide or standard for snow supporting structures.

1.4 Research Tasks

The process of snow load verification and SSS performance monitoring was originally proposed as a three-task scope of work. In summer of 2016, an additional scope of work item with an associated fee increase was added to the contract and is listed below as Task Four.

1.4.1 Task 1: Installation of Instrumentation on SSS

This task focused on the selection and installation of an array of transducers capable of monitoring the primary parameters needed to accomplish the research objectives. The task also included observations of the newly installed 87 SSS deployment during the winter of 2012-2013 to assess snow distribution across the site in order to provide a basis for selection of which SSS to instrument and monitor for the duration of the project. Originally, this task proposed instrumenting two different SSS, one stand-alone (not adjacent to any other SSS) and one end-unit of a double SSS grouping (side-by-side pair). However, it was decided early-on in the beginning of the project to instrument only one SSS that was part of a double SSS arrangement so that a more dense data field could be obtained: rather than distributing the transducer package across two units, it was used on a single SSS unit to improve the resolution of the experimentally measured physical quantities of interest (e.g. snow pressure, snow depth, etc.).

1.4.2 Task 2: Collect Data for Two Winter Seasons and Visually Evaluate Site for Three Summers

This task included the continuous monitoring and recording of experimental data produced by the instrumentation for two winter seasons, originally planned for winters 2013-2014 and 2014-2015. Because of on-going construction activities during the summer of 2013 by the original SSS installation contractor to address foundation installation errors, the research project was delayed one year and a one-year no-cost extension was granted. This task also included visual inspection of the 87 SSS for any signs of distress or issues requiring maintenance over a period of three summers including 2014, 2015 and 2016. The visual inspections focused on the SSS micropile foundations, foundation connection to SSS, structural steel members, and welded and bolted connections.

1.4.3 Task 3: Data Analysis and Develop Final Deliverables

A complete evaluation of all collected experimental data for trends and for comparison with snow pressure effects predicted by theory was performed in this task. This included comparison of average snow pressures calculated for both winter seasons with those derived by analytical expressions in the Swiss Guide and an additional theoretical model. Also performed was an evaluation of the variation of experimental snow pressure across the width dimension of the SSS along with a comparison to theoretical variation. The final aspect of this task is organization and compilation of all of the research results into a final research project report.

1.4.4 Task 4: Addendum to Original Scope, Installation of Glide Shoes and Moisture Sensors

An addendum to the scope of work was approved in 2016 for the fabrication, installation, and data recording of instrumentation to monitor snowpack movement relative to the ground surface ("glide"). This included sensors to measure snowpack displacement and soil moisture sensors to evaluate whether water was present at the ground surface for winter season 2017. Analysis of this additional experimental data fell under Task 3 above. Unfortunately this task was not entirely successful. The additional instrumentation was installed in the Fall of 2016 and was operational at that point. However, a complete loss of system power in early December prevented the collection of any data over the winter 2017 season. A request to access the site was submitted to the USFS Jackson Ranger District in December and again in January, but access was denied. Therefore, it was not possible to trouble-shoot the instrumentation via an onsite visit.

1.5 Outcomes

This research provides invaluable information on the applicability of the Swiss Guide for design of snow supporting structure projects within the United States. Specifically, because the use of constructed defense to mitigate avalanche danger along transportation corridors is novel, as is the NEPA-conforming site layout scheme, the results will help to inform future WYDOT and other State DOTs constructed defense projects. Results of the work will also help to build a foundation for the development of a domestic design specification or guide that can be utilized by other practicing engineers.

1.6 Report Organization

This report includes seven chapters, each of which is described in overview below.

- Chapter 1 provides an introduction to the project, including motivation for it, objectives of the work, and the research tasks identified to accomplish the objectives.

- Chapter 2 provides the necessary background information that forms the basis for interpretation and comparison of the experimentally measured parameters of interest. This includes an overview of basic snow mechanics as it relates to snow pressure, the Swiss Guide snow pressure provisions, and also an additional analytical snow pressure formulation developed by the leading researcher in the area of snow pressure.
- Chapter 3 provides an in-depth description of the experimental design of the project including decision-making on which structure to monitor, and selection and installation of transducers to measure the key experimental parameters of interest.
- Chapter 4 presents the results of the experimental portion of the project including interpretation of the results within the context of snow pressure theory.
- Chapter 5 gives a comparison of the experimental results with expected values given by the Swiss Guide and the additional analytical model.
- Chapter 6 provides a summary of all visual inspections performed during summertime to evaluate the performance of the SSS facility.
- Chapter 7 provides a summary of the research work, conclusions, and recommendations for future research work.

CHAPTER 2: THEORETICAL FRAMEWORK

2.1 Snow Pressure Theory Basics

2.1.1 Overview

Snow pressures acting on a rigid snow supporting structure located in an avalanche starting zone are caused by the interruption of snowpack deformations immediately uphill of the structure. Specifically, two different types of down-slope movements occur: internal *creep* deformation within the thickness of the snowpack layer, and rigid-body motion of the entire block of snowpack relative to the ground surface – *glide*. In its most basic form, the down-slope snow pressure component is in the form of an increasing pressure with increasing density and depth of material: *"ρ x g x H";* this form of pressure calculation is ubiquitous within physics and civil engineering. The determination of the down-slope pressure is also analogous to the lateral earth pressure problem where the tendency for lateral spreading of a material under its own weight or under the influence of another force depends on basic material characteristics such as cohesion and friction. In the snow pressure problem, the down-slope pressure depends on the internal creep deformation within the height of snowpack and movement of the entire snowpack relative to the ground surface, and snow is assumed to have a viscoelastic material response. Viscoelastic behavior is characterized as a combination of elastic material response (material stresses proportional to deformations) and viscous or fluid-like response (material stresses proportional to velocity).

Although snow creep is a complex, time-dependent phenomenon, the fundamental feature is increasing snow pressure with increasing slope angle (steepness) and snow density (see figure 2). The snowpack glide phenomenon is influenced by the roughness of the snowpack-to-ground interface: a relatively smooth ground surface allows the snowpack to slide downhill unrestricted once the ground surface temperature rises above freezing, while a very rough surface with many large obstacles such as boulders and bushes limits the movement of the snowpack along the slope. Also influencing the rate of glide and hence snow pressure is the orientation of the slope with respect to the sun, or the "solar exposure". Slopes facing primarily north or northeast or northwest will have less total solar warming during the daytime and therefore less glide. Sites with a more southern facing slope experience higher glide rates due to the greater amount of solar energy incident on the snow surface.

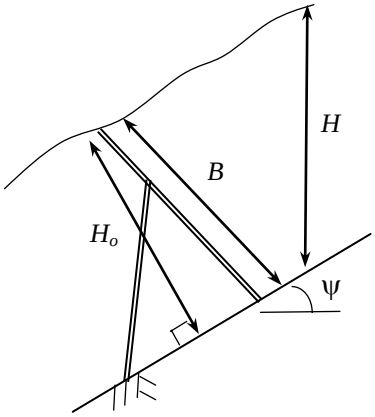

H = vertical snow height

H_o = snow height measured normal to slope

B = height of SSS along grate surface

ψ = slope angle

Figure 2 Definition of basic SSS geometry

Snow pressure equations in the Swiss Guide and analytical expressions by others provide a solution describing the *average* slope-parallel snow pressure to be applied to a fixed object of infinite width (along contour) supporting an uphill snowpack. This pressure is assumed to be uniformly distributed across the entire height of a structure even though finite-element studies and experimental results indicate that the snow pressure varies from zero at the upper free surface of the snowpack to a maximum pressure at around mid-height of the structure and then back to a smaller non-zero value near the ground surface (Larsen 1984). This is depicted in figure 3 below, which portrays a non-linear form of snow pressure variation with height, and also the average snow pressure given by equations and used in design.

No closed-form solutions for snow pressure variation with height in the snowpack exist, and therefore it is not possible to compare the theoretical and experimental maximum snow pressure acting on a SSS. However, while use of an average uniform snow pressure and the resulting total snow force is adequate for overall SSS reaction calculations for foundation design, individual member design requires quantification of maximum pressure effects since these local maximum pressures govern the internal axial force, shear force, and bending moment present in a specific component (e.g. SSS crossbeam). Therefore, examination of localized maximum snow pressures and a comparison to the average pressure is an important aspect of this research.

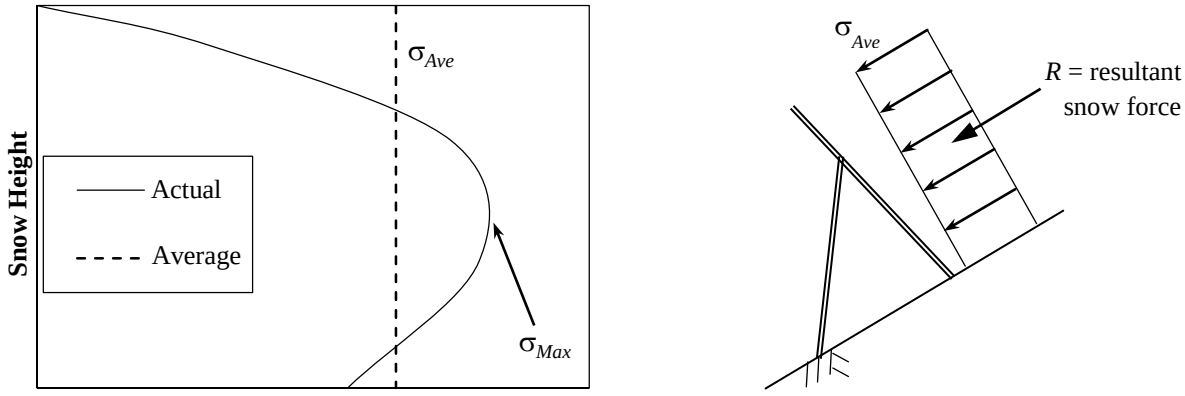

(a) Slope-parallel snow pressure
(b) Design uniform snow pressure and resultant

Figure 3 Actual versus average (design) slope-parallel snow pressure

2.1.2 End-Effects

The snow pressure equations presented previously apply to an infinitely wide SSS, where "width" is across slope and along a contour line. Under this scenario, snowpack movement down-slope is completely arrested by the infinitely wide SSS. When a SSS has a finite dimension and a free edge with no adjoining SSS, the snowpack will tend to move laterally around the SSS and down the slope. This phenomenon can be visualized by considering an obstruction placed in the middle of a stream and the tendency for the moving water to go around either edge of the obstacle. The movement of snow around the free edge increases the snow pressures imparted to a SSS in the "end-effect region". This increase in effective pressure can be extremely large depending on the open, clear distance to the next adjoining obstacle (i.e. another SSS). In the Swiss Guide, the increase in snow pressure at the end-effect region as compared to pressures in the middle of a SSS can be on the order of 100 percent to 500 percent.

During the original design of the Milepost 151 facility, a layout of SSS with somewhat irregular appearance was chosen, with small groupings of individual SSS rather than long continuous rows of SSS as it the practice in Europe. Although the continuous rows arrangement is overall more efficient because the design snow pressures away from the ends of rows are much lower than at the end-effect regions, it adds a visual element to the landscape that is foreign and makes SSS more visible from a distance. At the 151 Milepost site, design of a single SSS unit that could operate stand-alone and not near any other SSS was selected since the layout of SSS included many single SSS not near other SSS. Thus, all SSS at the Milepost 151 site were designed for the increased end-effect pressures acting at either free edge of the SSS and this approach resulted in SSS being over-designed where they were placed in groups of two or more SSS units. One of the key parameters of interest in this research was variation of snow pressure across the width of a SSS, from the center region away from the free edge to the end-effect region at the side of a SSS without an adjoining SSS. It is also important to note that the increased end-effect pressure is expected to be more pronounced when glide motions are greatest since the increase results from movement of snow cover around the free edge of the SSS. Thus, the differences between pressures occurring interior to the SSS and those at the free edge should be greatest in the springtime when higher average daytime temperatures occur (i.e. when high glide rates are present).

2.2 Swiss Design Guide Snow Pressure

2.2.1 Average Snow Pressure Without End-Effects

The Swiss Design Guide has been, and continues to be, the worldwide *de-facto* design specification for implementation of snow supporting structures. This document is the only comprehensive source for information on how rigid and flexible snow supporting structures should be designed to withstand the snow loads imposed within an avalanche starting zone. The pressures are given as a function of: depth-averaged snow density, ρ, snowpack height, H, slope inclination, ψ, solar exposure (i.e. aspect or orientation with respect to cardinal directions), and ground surface roughness characteristics. To a large extent the theoretical basis for snow pressures in the Swiss Guide is work done in the mid-1900s by Haefeli (1948), and a significant portion of the design guidance is based on empirical data and information from Europe. Two separate factors in the Swiss Guide account for the creep and glide motions of snow and are the creep factor, K, and the glide factor, N. Equation (1) is the Swiss Guide expression for slope-parallel resultant snow force per unit width (along slope contour) of structure, S_N:

— — — (1)

where,

ρ = density of snow (slug/ft^3 or kg/m^3)
g = acceleration of gravity (ft/sec^2 or m/sec^2)
H = vertical snow height (ft or m)
K = creep factor (no units)
N = glide factor (no units).

In order to determine an average slope-parallel snow pressure, $\sigma_{Ave,}$ the above snow resultant force is assumed distributed uniformly over the height of the SSS, where that height H_o is

measured normal to the slope as shown in figure 2. From the basic geometry shown, $H_o = H$ x *cosine*(ψ) and average snow pressure is by equation (2):

— ——— (2)

If snow height measured normal to the slope, H_o, is used in the snow pressure formula, equation (2) takes the following form given by equation (3):

— ——— (3)

Snow density is prescribed in the Swiss Guide as a function of altitude above a reference altitude of 4921 ft (1500 meters). At the reference altitude, the Swiss Guide assumes a uniform snow density of $\rho = 16.90$ lb/ft^3 ($\rho = 270$ kg/m^3) which, expressed as a fraction of the unit weight of water, is $\rho = 0.270$. This basic snow density value is increased with an altitude factor, f_c, which is determined by equations (4) or (5):

(ft) (4)

— (m) (5)

where,

Z = altitude above sea level, $4921.26 \leq Z \leq 9842.5$ (ft), for Equation (4)

Z = altitude above sea level, $1500 \leq Z \leq 3000$ (m), for Equation (5)

The creep factor, K, is given in the Swiss Guide as a function of slope angle, ψ, and depth-average snowpack density, ρ. Table 1 below provides the data from the Swiss Guide for $K/sin(2\psi)$. From the table it is evident that the creep phenomenon increases with increasing snow density and slope angle. For the Milepost 151 site, the Swiss Guide indicated a snowpack density of $\rho = 0.31$ based on site elevation, and the slope angle at the instrumented SSS was measured as $\psi = 37°$.

Table 1 Swiss Guide Creep factor, K, function of snow density, ρ, and slope angle, ψ

ρ	0.20	0.30	0.40	0.50	0.60
$K/sin(2\psi)$	0.70	0.76	0.83	0.92	1.05

Source: Adapted from FOEN (2006)

The glide factor, N, is presented in the Swiss Guide for four basic categories of ground surface roughness characteristics and solar exposure. The lowest glide factor is $N = 1.2$ which corresponds to a slope surface with coarse scree and boulders with diameter of at least 12 inch (25.4 mm) and primarily northern solar exposure. The highest glide factor in the Swiss Guide is $N = 3.2$ which corresponds to slopes with long-bladed compact grass cover with scree mixed with earth and a more southern solar exposure. Examination of the tabulated values of N in the Swiss Guide indicates that the solar exposure influence is only approximately a 20 percent factor going from northern to southern exposure. Ground surface characteristics on the other hand increase glide by a factor of a little more than two going from the roughest to smoothest surface

condition. At the Milepost 151 site, the solar exposure is due west (worst case) and the ground is mostly free of any large objects and has long-bladed smooth grass cover. During design of the Milepost 151 facility a glide factor of $N = 3$ was assumed (Swiss Guide stipulates interpolation between glide factors for conditions between the four classes of ground surface roughness).

2.2.2 Average Snow Pressure in End-Effect Region

An end-effect factor, f_R, is stipulated in the Swiss Guide and increases the average snow pressure by the addition of an end-effect snow force, S_R. The actual variation of snow pressure across the width of a SSS isolated by itself in a free snow field is depicted in figure 4 along with the typical stepped uniform distribution used in design. The end-effect factor in the Swiss Guide is determined by equations (6) and (7) given below. It is based on the separation distance between individual SSS, A, and varies from $f_R = 0$ for no separation (i.e. A=0) to $f_R = 5$ for a SSS with infinite distance to the next adjacent SSS (i.e. A=∞) and with glide factor $N = 3.2$. Equations (8) and (9) indicate how the end-effect factor is applied by the Swiss Guide to calculate the total snow force acting in the end-effect region, R_N: the additional end-effect snow force, S_R, is added to the basic snow force resultant without end-effects, S_N. The Swiss Guide indicates that average slope-parallel pressures at the end-effect region of a SSS with no adjacent SSS are six times larger than those for an infinitely wide SSS (no end-effects). For the Milepost 151 site, the end-effect factor per the Swiss Guide used in design of the SSS was $f_R = 4.75$ (by right-hand side limit of equation (6) or (7) with N=3).

—— [A in ft] (6)

—— [A in m] (7)

(8)

(9)

where,

S_R = additional resultant force in the end-effect region due to end-effects

R_N = total resultant snow force in the end-effect region

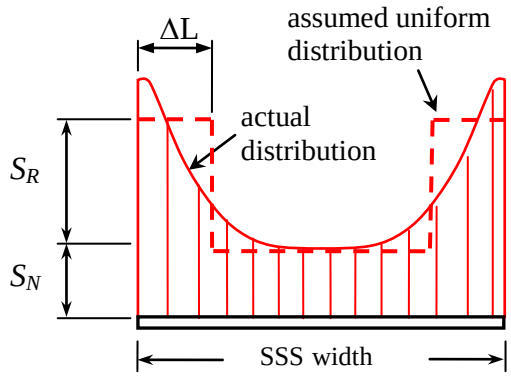

Figure 4 Lateral distribution of snow pressures on isolated SSS

2.3 McClung Continuum Analytical Model

2.3.1 Average Snow Pressures Without End-Effects

An alternative analytical solution to the Swiss Guide model for average snow pressures away from end-effect regions has been presented by McClung (McClung 1982, McClung et al. 1983, Larsen et al. 1984, McClung & Larsen 1989, McClung 1993). The "McClung Model", developed based on a continuum mechanics approach, has been shown to yield excellent agreement when theoretical pressures were compared against snow pressure data from Switzerland and Norway (McClung 1993). The slope-parallel resultant snow force per unit width (along slope contour) of structure is given by McClung as equation (10) below. Note that this equation utilizes the snow height as measured normal to the ground, H_o.

(10)

where,

L/H_o = factor accounting for boundary conditions of SSS grate surface; if no slip of snow cover with respect to surface occurs, L/H_o is by equation (11) below (McClung 1993),

D/H_o = stagnation depth, related to the glide factor N by equation (12) (McClung 1993),

(11)

(12)

Similar to the above for the Swiss Guide, converting the resultant snow force per SSS width to an average (uniform) pressure over the SSS height, the average snow pressure is:

(13)

2.3.2 Average Snow Pressure in End-Effect Region

Unlike the Swiss Guide, the analytical model for snow pressure effects presented by McClung does not include expressions for determination of end-effect region pressures. Thus, in later sections of this report where experimental and analytical end-effect pressures are compared, it is only for the Swiss Guide theoretical model.

CHAPTER 3: SSS INSTRUMENTATION PACKAGE

3.1 Selection of SSS to Instrument and Monitor

The selection of which SSS to instrument was a critical aspect of the planning process of the project. Ideally, a location with the biggest and most consistent snowpack depth was desired. Photographs of the Milepost 151 Site from the valley floor were taken during the peak of the 2013-2014 winter season to assess the distribution of snow across the site and to determine which SSS experienced the highest snow deposition. Figure 5 below shows a zoomed-in view of the upper reaches of the site and the three locations of SSS considered for instrumentation. Row "A" as shown in the figure was identified as the most appropriate site based on snowpack present at the time of the photo as also based on the relatively larger unsupported tile of snowpack uphill and to the viewer's left from that row (highlighted as a white region with dots on the photograph). This large tile of unsupported snow would be expected to induce the largest snow pressures, and in fact, a small avalanche was released from this region in January of 2015, striking the SSS immediately below it. The actual SSS that was instrumented corresponds to structure number 74 from the construction documents. A plan view of the Milepost 151 facility is provided in figure 6 along with the SSS units considered for instrumentation.

3.2 Data Acquisition and Transducer Details

3.2.1 Pressure Transducers

One of the key snow parameters of interest was pressure exerted by the snowpack on the SSS grate surface (series of steel crossbeams). Originally, it was proposed to use strain gages affixed to steel crossbeams and to the micropile foundation bars to allow for determination of SSS member forces, which could then be used to back-calculate snow loads acting on the SSS. However, during final experimental design, the idea of measuring snow pressure directly with pressure transducers mounted to the SSS grate surface was determined to be not only feasible, but also a much more direct measure of snow loads – pressure measurements can easily be converted to force quantities using the surface area.

Geokon, Inc. Model 4800 vibrating wire pressure cells (PC) were selected based on their excellent track-record for long-term stability measuring pressure. They are composed of six by ten inch rectangular steel flat plates welded together with a fluid filled cavity that is connected to a vibrating wire transducer, which converts changes in internal pressure to an electrical signal. The full-scale capability of the pressure cells was approximately 10 psi. Figure 7 below shows a PC mounted with a one-quarter inch thick steel backing plate and on the uppermost crossbeam of the instrumented SSS. Figures 8 and 9 illustrate the naming convention and locations of all twenty PCs. Four "columns" of PCs were arranged across the width (parallel to contour line) with column one at the southernmost free edge of the SSS, column four at the opposite side, and columns two and three at the interior of the SSS. Experimental snow pressure data presented in subsequent sections of this report is also grouped by row number, where the first row corresponds to the lowest crossbeam, and the fifth row corresponds to the uppermost crossbeam (figure 9).

Each PC also contains a thermistor to record temperature at the PC, and thus 20 temperature sensors were also distributed across the SSS grate surface which allowed for determination of temperature within snowpack height.

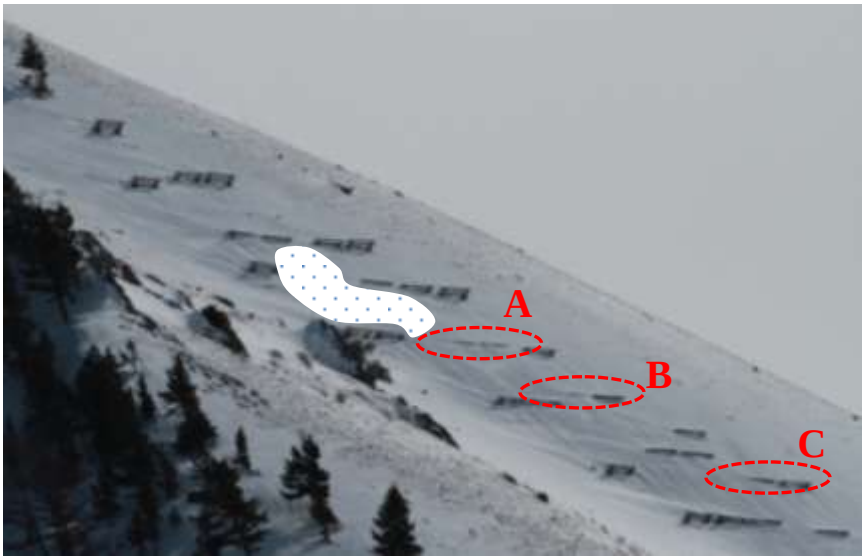

Figure 5 Photograph of SSS deployment and SSS considered for instrumentation

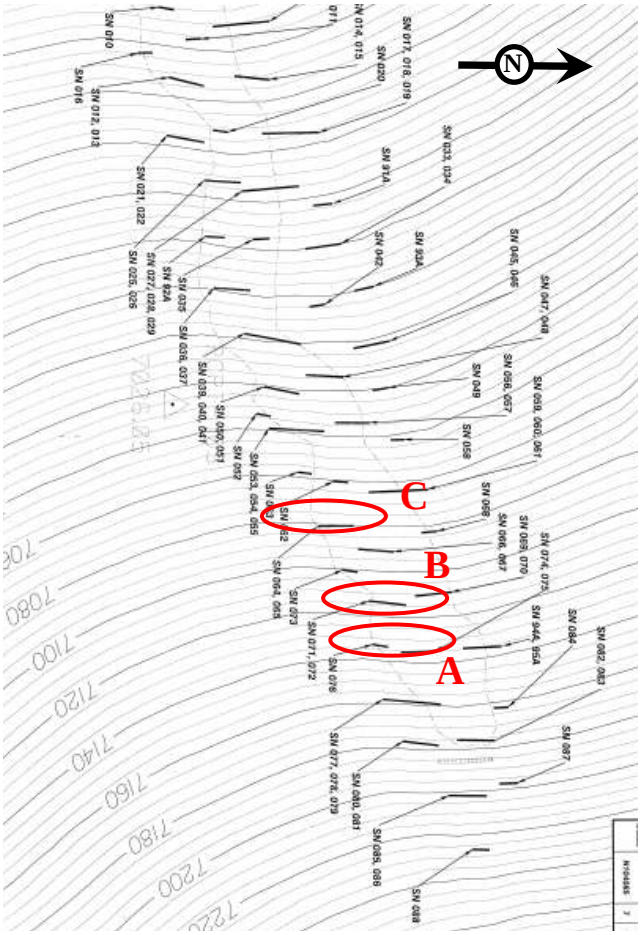

Source: WYDOT

Figure 6 Plan view of deployment and SSS considered for instrumentation

Figure 7 Pressure cell 16 mounted on uppermost crossbeam

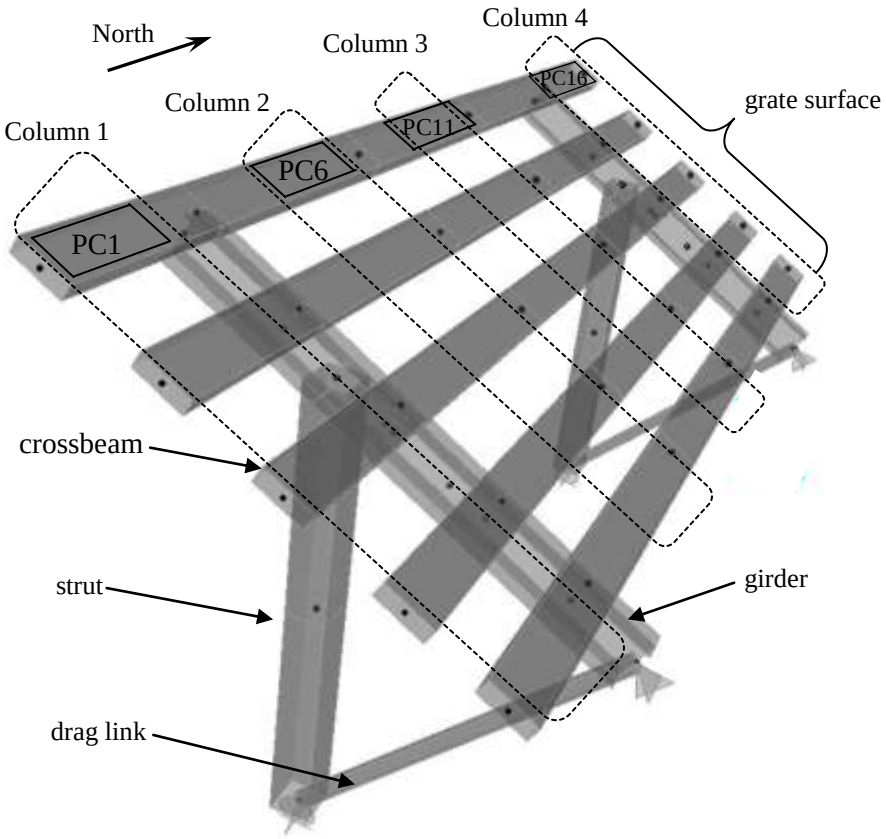

Figure 8 Pressure cell layout on SSS – Isometric view

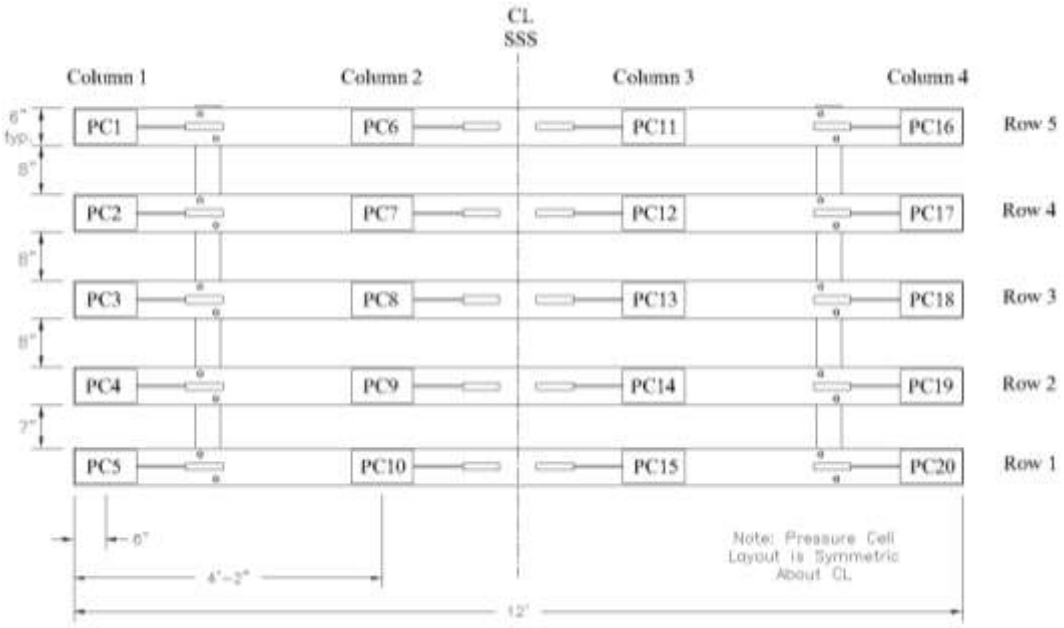

Figure 9 Pressure cell layout on SSS – Perpendicular view of grate surface

3.2.2 Snow Depth Sensors

Three ultrasonic snow depth sensors were installed across the width of the SSS to monitor snowpack depth immediately uphill of the SSS grate surface. Each of the sensors was mounted on a cantilevered mast that was attached to the SSS grate surface, as visible in figure 10. The location of each snow depth sensor across the width of the SSS was based on available space on the crossbeams once pressure cells were installed. Two sensors were located 30 inch (762 mm) inboard from the end of the crossbeams, one on each side of the SSS. The third sensor was located at exactly the middle of the SSS. The sensors used were Judd Communications ultrasonic depth sensors and operate by sending an ultrasonic pulse downwards towards the snowpack surface. The wave reflects back off the snowpack surface and the total travel time is used to calculate distance between the sensor and the surface of snow. Where snow height is used in calculation of snow pressure later in this report, the heights used are based on pressure cell location, e.g. column one or two, etc. For column one, the snow depth sensor #3 (see figure 10) data was used. For column two pressure cells, data from snow depth sensors #2 and #3 were averaged to get snow height. For column three, data from snow depth sensors #2 and #1 were averaged for snow height, while snow sensor #1 was used for snow depth at column four.

3.2.3 Vibrating Wire Strain Gages

In order to provide a check on the accuracy of snow pressure data recorded by pressure cells, a series of vibrating wire strain gages (VWSG) were mounted to parts of the SSS to monitor internal normal strains, which can be used to determine internal stresses. Based on static equilibrium of a SSS, knowledge of the axial compression force within each strut can be used to back-calculate the snow pressure resultant force. Alternatively, with snow pressure resultant force determined from pressure cell data (details in section 4.5 of this report), the required internal axial force in the struts based on equilibrium considerations can be calculated. Based on this approach, each strut was instrumented with two VWSG just above mid-height of the strut on the front and back sides of the strut when the SSS is viewed from the side (see figure 11). This

location (front and back) was selected because of the top and bottom boundary conditions of the strut in a plane containing the strut and the girder: the top and bottom can be considered pinned connections which eliminates the possibility of strut internal moments influencing the measured normal strains. That is, with these locations of VWSG, any measured strains should be due to pure axial force and not moment. Figure 12 shows a photograph of the north strut with the VWSG on the front face covered by an aluminum angle to protect it from the elements.

Figure 10 Photograph of SSS with pressure cells and snow depth transducers

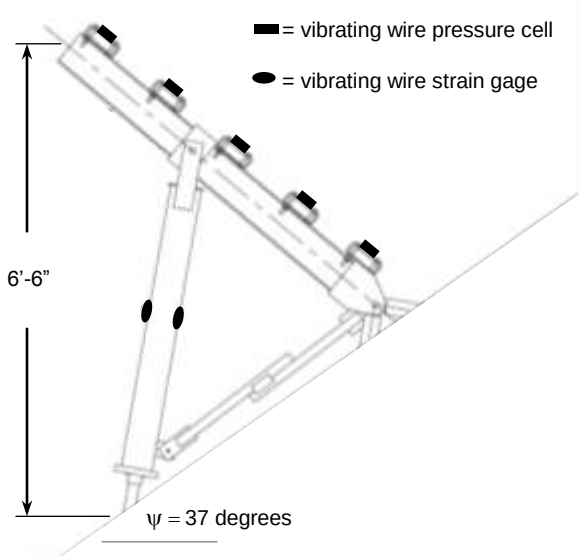

Figure 11: SSS with strain gage & pressure cell locations

3.2.4 Glide Shoes and Moisture Sensors

During the spring of 2016, after two seasons of experimental data had been obtained, a change of scope and contract extension with an associated fee increase was requested to allow for the addition of hardware to monitor glide movements. Other researchers have recently reported on the successful implementation of transducers to measure how much downhill movement the snow cover experiences during springtime when thawing of the snow allows for the glide phenomenon to occur (De Biagi et al. 2013). The basic transducer details include a linear motion sensor that has a long wire wrapped around a drum, and the wire connected to a metal "glide shoe" that is placed on the ground surface. The glide shoe has vertical fins that cause it to interlock with the snowpack above it. Any slipping of the snowpack with respect to the ground surface causes the glide shoe to move, which in turns pulls more wire off of the drum. The circular motion of the drum is converted to an electrical signal that can be used to determine linear displacement. Celesco SR1V string potentiometers were used along with fabricated steel glide shoes. Three glide shoes were fabricated and installed approximately six feet (1.829 m) upslope from the instrumented SSS. Two were installed five feet (1.524 m) outward (laterally) from the middle of the SSS while the third was installed in the open slope area immediately to the northern free edge of the SSS to monitor snowpack movements where it is not supported by the SSS.

Three Campbell Scientific CS655 water content reflectometers were installed along the glide shoes to measure the presence of water at the ground surface. One sensor was buried approximately one to two inch (25 to 50 mm) below the ground surface and adjacent to each glide shoe. Because glide movement is correlated with the unlocking of the snowpack from the ground surface and movement along the surface lubricated with water, the moisture sensors are used to confirm the presence of water when glide motions are observed in the data record.

3.2.5 Data Acquisition System, Remote Access, and Installation

Electrical signal conditioning and data recording was accomplished using hardware and software provided by Geokon, Inc. A Campbell Scientific model CR800 data logger was used to provide electrical excitation for snow sensors, strain gages, and pressure cells. A cellular data modem was connected to the logger and allowed for remote access to the data so that no trips to the site were required during winter. The system was powered by a deep cycle 12-volt battery that was charged by a 20 watt solar panel. The frequency of data logging was set to hourly, and the system began logging data on September 24, 2014. The entire data acquisition system and battery were housed in a weather-proof lock box, as shown in figure 13. Cylinders of desiccant material were enclosed in the box to help prevent collection of moisture inside that could cause corrosion of electrical circuits.

Figure 12 Photograph of SSS strut and girder with vibrating wire strain gage

Figure 13 Photograph of SSS with data acquisition lock-box

CHAPTER 4: EXPERIMENTAL RESULTS

4.1 Introduction

The behavior of snow cover can be envisioned as both that of a solid and fluid, and physical properties change continuously over the course of a winter season. Snow is also heterogeneous with properties varying spatially at any one instant. After fresh snow has fallen it begins to densify under the presence of gravity and other environmental factors such as temperature and wind. A snowpack has the ability to resist both tensile and compressive stresses and can span across gaps in a manner similar to the way a piece of wood lumber can span an opening. Because of this, and the fact that creep and glide of the snow is not uniform in the fall-line and across the slope, a planar surface supporting snow may not have snow in direct contact at all areas of the surface. Moreover, even if uniform contact does occur, the spatial variation of snow properties can influence the snow pressures imparted at different regions of the surface. With these concepts in mind, it is reasonable that snow pressures recorded by adjacent PCs can vary significantly at any given instant. For example, glide motion of the snowpack can cause rigid-body movement of the snowpack such that it is no longer in contact with some areas of the SSS surface while it is bearing at other regions of the SSS grate surface. Under this scenario, a pressure cell in one column can experience very high pressures while one in the adjacent experiences little pressure at the same instant. This phenomenon was in fact observed in the pressure cell data. Thus, an approach where two-week periods of data were grouped together was used, and the maximums over the two-week period for all experimentally measured parameters are plotted even though they may have occurred hours or days apart.

4.2 Snow Height by Ultrasonic Snow Depth Sensors

Distance measurements recorded by snow depth sensors mounted to the SSS were used to derive snow height perpendicular to the ground, H_o. The ultrasonic snow sensors actually record distance to a reflecting surface from the sensor location rather than height of snow cover top surface from the ground. Thus, to determine snow height from the recorded sensor data, the readings of a sensor over the course of the winter are simply subtracted from the original reading obtained with no snow present. The change indicated by this resulting number is the snow cover height.

Snow sensor data for winter season 2015 are shown in figure 14. The maximum snowpack height for the season occurred on January 18th and was 72 inch (1.830 m) at snow depth sensor #1 (northernmost sensor). Maximum heights at sensors #2 and #3 were 66 inch (1.676 m) and 71 inch (1.803 m), respectively. From January 1st through the end of the winter season, three major snow events are indicated in the snow sensor records: January 4th, January 17th, and February 4th. These dates correlate exactly with recorded snowfall events from the town of Jackson and Jackson Hole Mountain resort. The indicated snowpack height on about March 7th also correlates with a measured snow cover depth of about four feet (1.22 m), which was observed during a visit to the site for snow sampling. Because of the very close agreement in snow depth between the three sensors, only one of the sensor data signal is shown in subsequent sections where correlations between snow height and other physical phenomena are being made. However, where snow height is used in calculations, the snow heights derived as described in Section 3.2.2 previously are used.

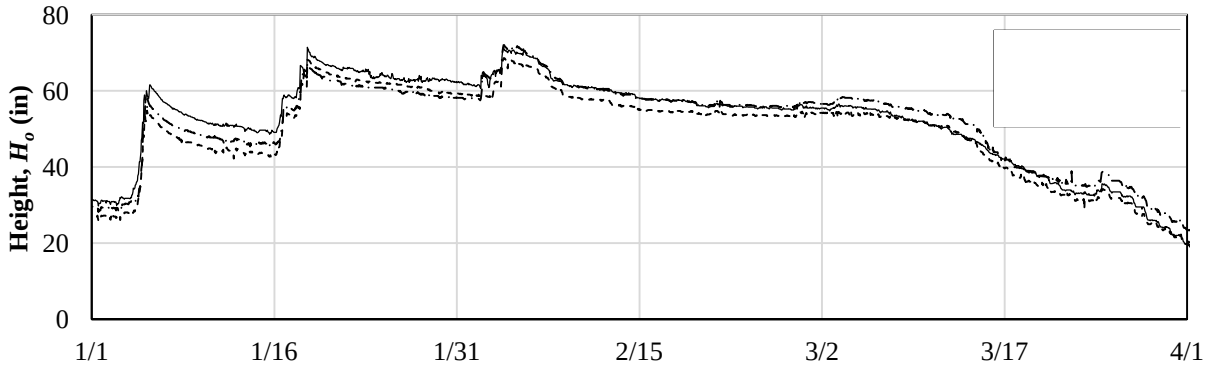

Figure 14 Snow height, H_o, recorded at the instrumented SSS for winter 2015

Snow height data for winter season 2016 is provided in figure 15. Snow height was minimal until the third week of January when it reached to just over 50 inch (1.27 m). A large storm at the end of January increased the snow height to just over 60 inch (1.524 m), with a seasonal maximum height of H_o = 62 inch (1.575 m) recorded at snow sensor #3. This maximum snow height is two inch (50 mm) below the center of the top row (row five) of pressure cells and thus the recorded snow pressure signals, presented later in the report, indicate essentially no snow pressure at this height. After the peak snowpack height was attained at the end of January, no additional significant snow events occurred and the snowpack decreased in height for the rest of the winter season.

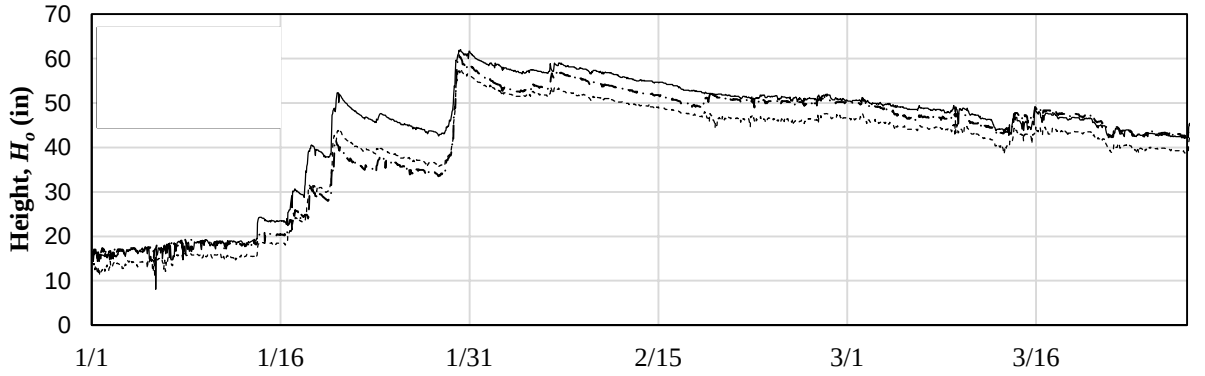

Figure 15 Snow height, H_o, recorded at the instrumented SSS for winter 2016

4.3 Snow Density

The density of snowpack varies with time over the course of a winter season and significantly influences the snow pressures exerted on a SSS. Freshly fallen snow can have a density on the order of 10 to 15 percent while late season heavily densified snow might have a density of 40 percent or more. Direct measurement of snowpack density requires either weighing a prism of snow and measuring its depth (this is the process used at SNOTEL sites) or weighing a sample of snow with a known volume. The Milepost 151 Site is located in a USFS Managed Big Game Winter Range area, which is closed to human access during the winter season. Because of this, it is not possible to measure snowpack density directly at the site, and estimates for snowpack density were made using data from the Granite Creek SNOTEL Site #497. This site has a similar west-facing aspect and is situated at an elevation of 6,770 ft (2063.5 m), which compares

favorably with the instrumented SSS elevation of approximately 7100 ft (2164.0 m). Unfortunately, one key difference between the sites is the snow deposition characteristics: the Milepost 151 snowpack is wind-loaded while this condition doesn't exist at the Granite Creek SNOTEL site. Consequently, the snowpack density at the Milepost 151 site is expected to be greater than that measured at the Granite Creek site.

So that a comparison of snowpack densities at the Milepost 151 and Granite Creek sites could be made, special permission to access the Milepost 151 site was granted by the USFS in March of 2016. InterAlpine Engineers' personnel hiked up to the instrumented SSS and a series of snowpack density measurements were made by collecting a sample of snowpack with known volume and then weighing the sample. Figure 16 below shows the instrumented SSS during the site visit for snowpack density sampling, and snow depth was approximately four feet (1.219 m). The spatial variation in the snow contact with the SSS grate surface described above is evident in the photo. A hollow aluminum cylinder with two inch (50 mm) diameter and three feet (0.914 m) in length was used to collect snow samples by pushing the cylinder into the snowpack at a number of different locations around the SSS. A series of samples were taken by pushing the cylinder into the snowpack immediately uphill of the SSS and perpendicular to the SSS supporting surface (i.e., perpendicular to the SSS crossbeams). A second series of samples was taken from a snow pit excavated adjacent to and on the uphill side of the SSS, along the fall line (perpendicular to a contour line). A photograph of the sample locations normal to the SSS supporting surface is provided in figure 17 below.

Snow sample data is provided in table 2. The average snow unit weight calculated from the four samples was 24.35 lb/ft^3, or expressed as a fraction of the unit weight of water (specific gravity), $\rho = 0.390$ (standard deviation = 0.036). The snowpack density recorded at the Granite Creek SNOTEL Site for the first week of March in 2016 was $\rho = 0.308$ (March 7th, 2016). The ratio of densities between the Milepost 151 site and the Granite Creek site is 1.27, and this is not surprising since the Milepost 151 snowpack should be of higher density because of wind loading. Based on this, in all subsequent calculations where snow density is used, data from the Granite Creek SNOTEL site was used, but increased by a factor of 1.27. It is acknowledged that this ratio will in actuality be variable depending on individual storm characteristics over a winter period (e.g. wind direction, wind speed, etc.), but without regular access to the Milepost 151 site no other viable option for snow density data is available for this research.

Table 2 Experimental snow density at Milepost 151 Site from March 7th, 2015

Sample No.	Weight (lb)	Density, ρ (lb/ft^3)
1	1.481	25.5
2	1.563	26.9
3	1.300	22.4
4	1.313	22.6

Snow density at the Granite Creek SNOTEL Site is presented in figures 18 and 19 for the 2015 and 2016 winter seasons, respectively. Density values shown do not include the 1.27 factor for the ratio between Milepost 151 and Granite Creek densities detailed above.

Figure 16 Instrumented SSS in March 2016 during snow density sampling

Figure 17 Snow sample locations during March 2016 snowpack density sampling

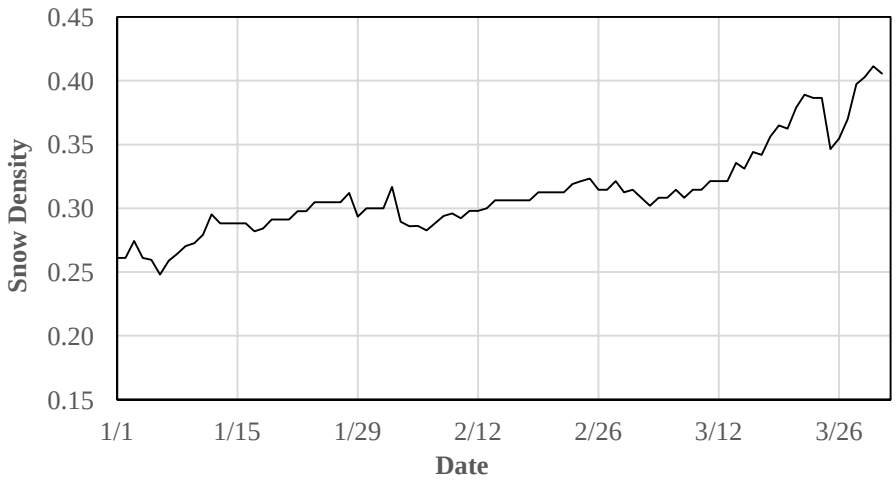

Figure 18 Snow density at Granite Creek SNOTEL Site #497 for 2015 winter season

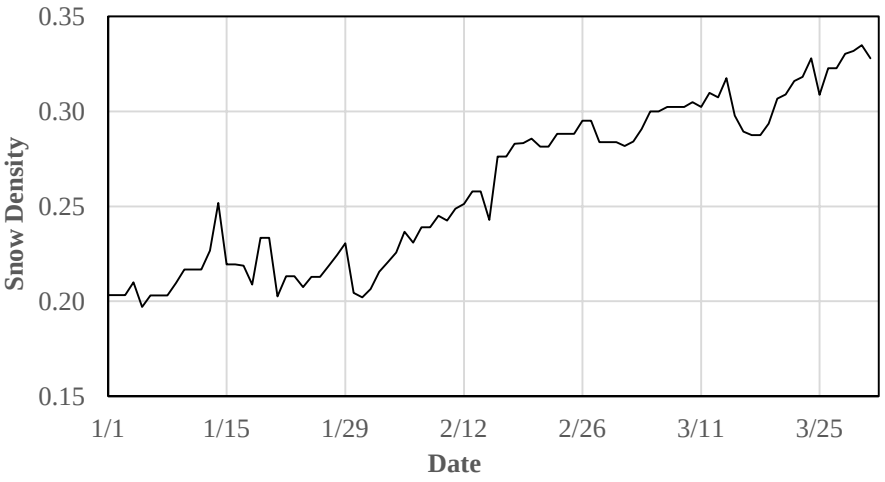

Figure 19 Snow density at Granite Creek SNOTEL Site #497 for 2016 winter season

4.4 Snow Pressures

Pressure cell recordings from each of the twenty vibrating pressure cell transducers were analyzed for winter seasons 2015 and 2016. It is again noted that snow is a highly heterogeneous material with both temporal and spatial variations in all physical properties. On a short time scale it exhibits properties of a solid, one of which is the ability to span or bridge across openings or gaps. Because of this, there is the possibility that a given pressure cell may experience a relatively high contact pressure from the snowpack while another pressure cell immediately adjacent (either on one side in the same row or above/below it in the same column but different row) registers almost no pressure whatsoever at the same instant. Thus, when examining snow pressure values for trends and correlations with the phenomena of interest, using maximum values of pressure over a time scale of days or even or weeks is more appropriate than using exactly time-concurrent data values. Aside from the presentation of pressure versus time graphs for each pressure cell, pressure data is grouped by maximum values for each PC that occur over a two-week period.

4.4.1 Vibrating Wire Pressure Cells Data Reduction

Pressure readings from vibrating wire pressure cells are influenced by all physical phenomena that act on the pressure cell including contact pressure from a snowpack, changes in ambient temperature (that cause thermal expansion/contraction of the steel pressure cell chamber), and changes in atmospheric pressure. Because snowpack pressure is desired, other sources of pressure change must be removed so that the snowpack only pressure signal can be obtained.

The most significant influence on pressure cell readings other than that caused by snowpack pressure is that due to barometric pressure variation. One-inch of mercury (inHg) barometric pressure change corresponds to 0.491 psi (3385 Pa). During the 2014-2015 monitoring season, the minimum barometric pressure was 29.27 inHg and the maximum was 30.58 inHg. This corresponds to a differential barometric pressure of 1.31 inHg, which corresponds to a 0.643 psi (4433 Pa) pressure differential. This is on the order of 10 percent of the maximum observed snowpack pressure during the 2015 winter season, and thus is significant. Recordings of atmospheric pressure for the Jackson Hole Airport obtained from http://www.wunderground.com were used to eliminate the atmospheric pressure signal from the pressure cell readings by simply subtracting the change in atmospheric from the pressure cell readings. Figure 20 below shows both the uncorrected and corrected pressure cell signals for barometric pressure influence correction for pressure cell five, 2015 winter season. The period shown from 1/10/15 to about 1/15/15 had an almost constant PC temperature of 29.3 °F (-1.5 °C), and thus the difference in the two pressure signals corresponds to primarily barometric pressure influence. It can be seen in the figure that once the barometric pressure signal was removed from the PC readings, a more constant pressure signal was obtained.

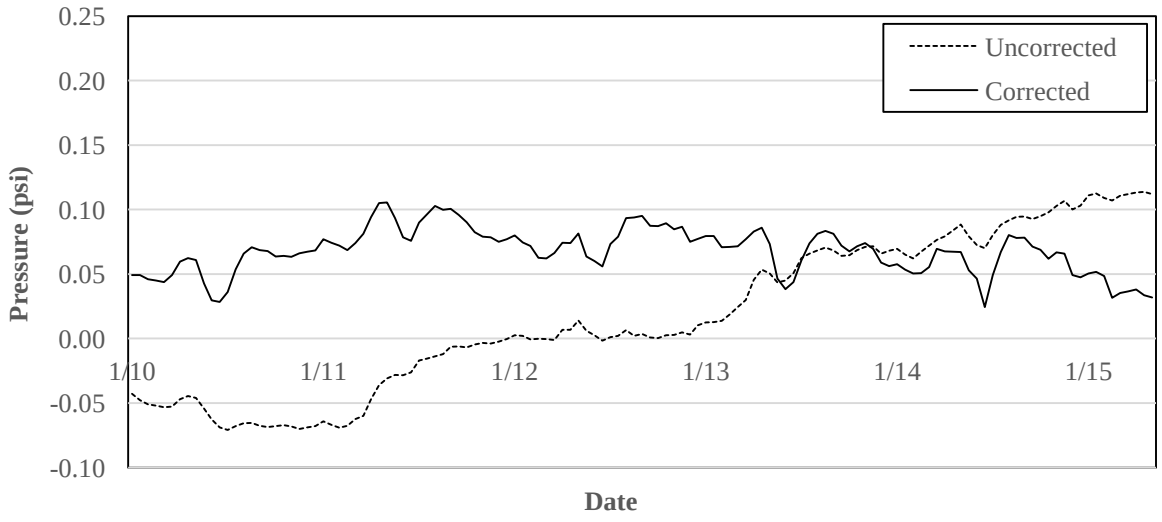

Figure 20 Influence of barometric pressure on pressure cell reading (pressure cell temperature constant)

The second modification to the pressure cell readings accounted for the influence of temperature change on pressure cell readings. Internal fluid pressure in the pressure cell transducer changes as the steel plates of the transducer heat during the daytime hours and cool at night. In order to account for this effect, pressure cell data was analyzed for periods when the barometric pressure was almost perfectly constant and when no snow was present. Under this condition, any changes in pressure cell reading are attributed to thermal effects. Pressure readings versus temperature change for this period were plotted (see figure 21) to obtain a temperature correction factor, “K”,

which is the slope of the line fit to the data. From the figure, it can be seen that the influence of thermal effects is very small – on the order of less than 0.1 psi (690 Pa) for the temperature range of +50 °F (10 °C) to 1.4 °F (-17 °C). Figure 22 illustrates the uncorrected, and corrected for temperature influence, PC signal for a period of almost constant barometric pressure for PC five and winter 2015. It can be seen that the corrected pressure signal is essentially constant at 0 psi (0 Pa) pressure which is what is desired since there is no snowpack pressure (no snow on SSS during this period) and because the barometric pressure was constant.

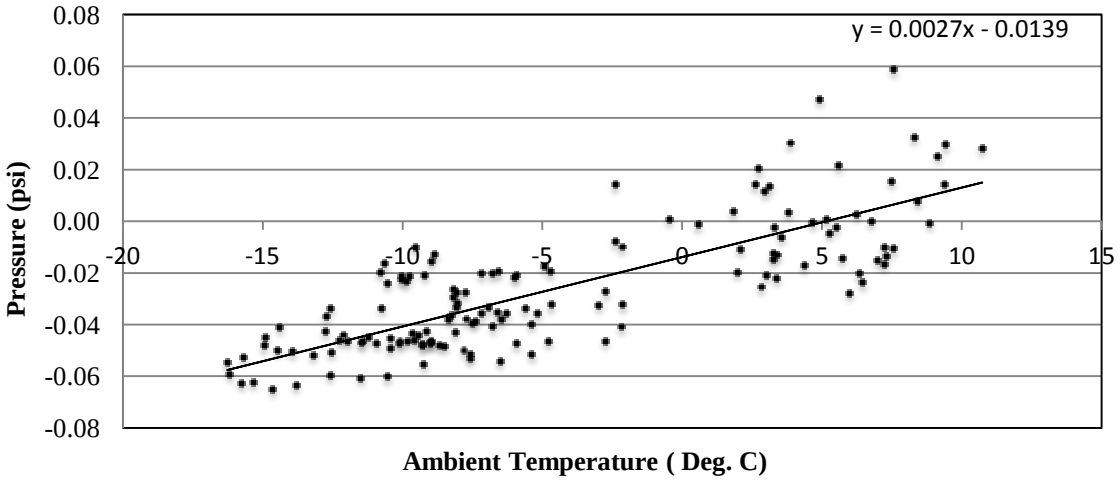

Figure 21 Influence of ambient temperature on pressure cell reading (barometric pressure constant)

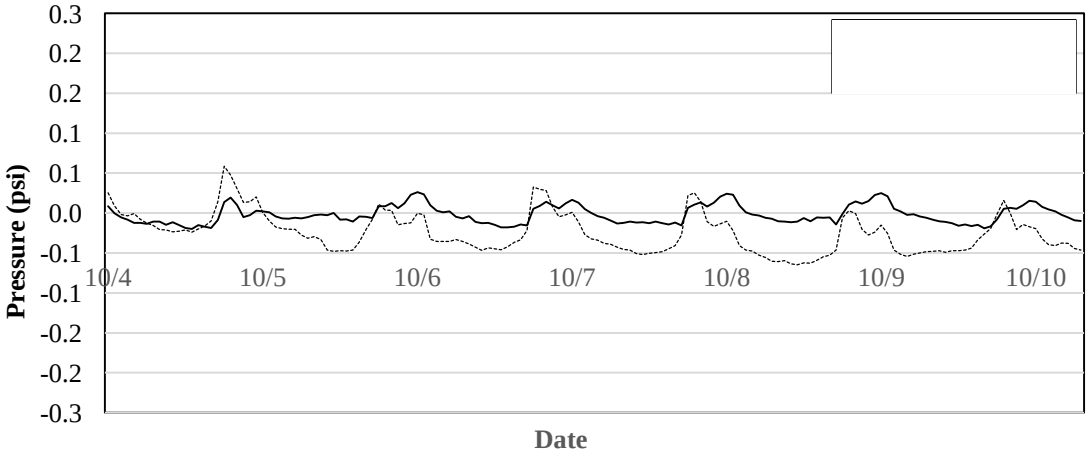

Figure 22 Pressure cell reading correction for temperature change (barometric pressure constant)

Figure 23 below illustrates pressure versus time for pressure cell five during the winter 2015 season. The raw, uncorrected pressure signal shows more frequent and larger scale increases and decreases which correspond to changes in the barometric pressure, while the corrected pressure signal more closely follows the zero pressure level during late fall of 2014 when little to no snowpack was present. Examination of the corrected pressure signal for the time period between late October and early December reveals a steadier signal with only minor fluctuations about the zero pressure level. It is believed that the minor changes in pressure during this period are due to deformations induced in the PC transducer by thermal expansion and contraction of the SSS itself. This influence on PC readings is not practical to eliminate because the thermal deformations of the steel SSS vary significantly depending on angle of the sun and hence thermal

gradients, and on depth of snowpack uphill of the SSS. Moreover, this influence constitutes a very small contribution to the total pressure reading (± 0.1 psi, ± 690 Pa)). The above-described modifications to raw PC recordings were performed for all PCs for both the 2015 and 2016 winter seasons, and subsequent sections of this report present only the final, corrected pressure data.

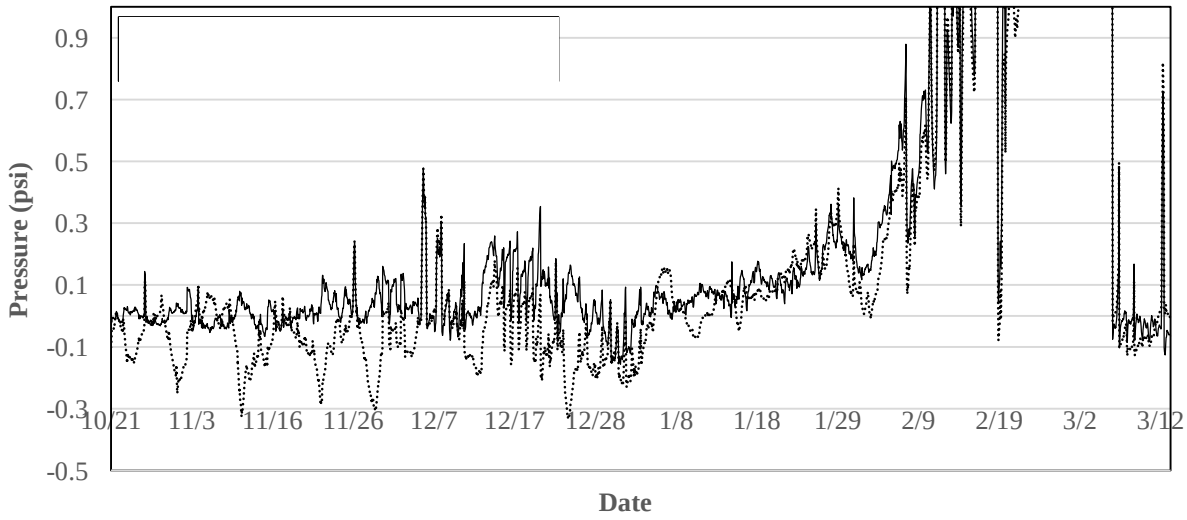

Figure 23 PC five raw (uncorrected) and snow pressure only (corrected) signals, winter 2015

4.4.2 Winter Season 2015 Snowpack Pressure Versus Time

Snow pressures recorded over the course of the 2015 winter season (January 1, 2015 through March 31, 2015) are shown plotted versus date for all twenty pressure cells in figures 25 through 29. Pressure graphs are grouped by column number. Also provided immediately below the column grouping figures is a graph of snowpack height normal to the ground surface as measured by the snow depth sensor #3 (nearest column one). Commentary on every single aspect of every pressure cell graph is not provided herein, but rather explanation of the salient features of the data is given.

The maximum recorded snow depth for the season was H_o = 72 inch (1.829 m), which occurred on January 18th. In figure 25 for column one, it can be seen that snow pressure intensity increases with downward distance from the snowpack top surface, (i.e. pressure increases with depth) PCs four and five have the least pressure and PCs three, four and five exhibit the greatest snow pressure. The highest recorded pressures occurred at PC four with a maximum of 4.72 psi (32.54 kPa) recorded on about February 26th. Considering the temporal variation of pressure, all pressures were relatively small at less than 1 psi (6.895 kPa) until early February, except for PC one. This PC experienced a spike in pressure on January 18th, which corresponds to a recorded small avalanche immediately upslope of the instrumented SSS that impacted the very top of the SSS. From figure 26, it can be seen that the majority of snow accumulated in the month of January and with the last major snowfall in the first week in February. After this time, daytime ambient temperatures increased significantly to well-above freezing and warming of the snowpack ensued. This is evident in the pressures at PCs two through five which show a rapid increase in recorded pressure which is associated with glide motion of the snow cover. During this period, the snow cover "unlocks" or releases from being frozen to the ground surface and

subsequently tends to move down the slope while water is present at the ground surface. In the evening as the temperature drops below freezing, the snowpack re-freezes to the ground and pressures drop with termination of glide motion. The pressure or stress is released once the glide motion stops due to creep relaxation within the snow and also because of the viscoelastic behavior of snow. The majority of the peak daily snow pressures are due to the velocity of snowpack movement (this is the "visco" aspect of snow response) and once this velocity decreases to zero, the pressure decreases. In order to illustrate the daily fluctuations of snow pressure with time, a shorter time-scale graph of pressure is provided for PC four in figure 24.

One last key feature from the column one pressure graphs is the apparent drop in snow pressure altogether after about March 5th. At this time a visit was made to the site to sample snow for snow density as described previously. It was noted during the visit that the snowpack was receding from being in contact with the SSS grate surface because of the very warm daytime ambient temperatures and the warming of the steel SSS. It is theorized that the rate of movement of snowpack was overcome by the rate of snowpack melting by the hot steel where the snowpack contacts the SSS.

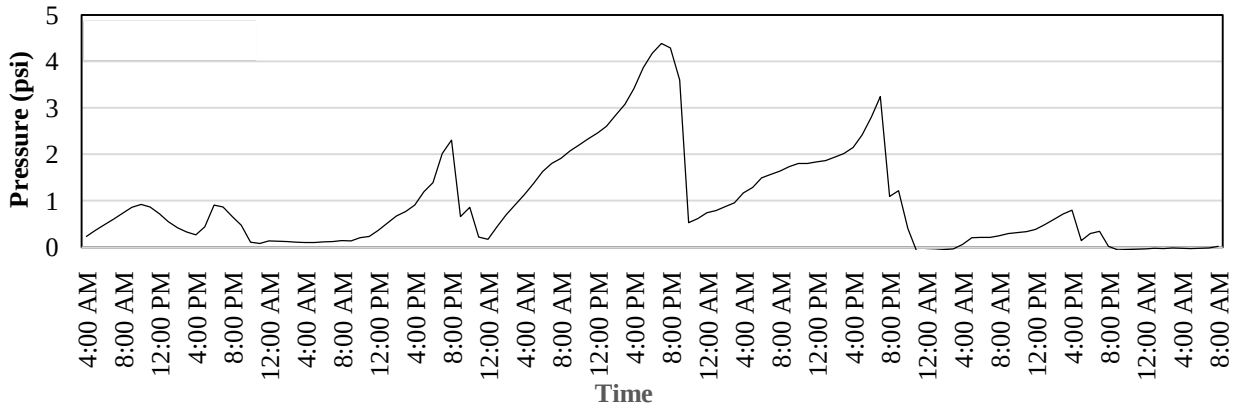

Figure 24 Daily fluctuation of snow pressure at PC#4 for five day period starting February 15th, 2015

Snow pressure graphs for PC columns two through four exhibit the same general characteristics as those detailed above for column one. However, it can be seen in figures 27 and 28 that maximum pressures recorded in columns two and three are significantly less than those in columns one and four. This is expected since they are located near the center of the SSS and away from the end-effect regions (this is analyzed in more detail in later sections of this report). Maximum seasonal snow pressures within columns two and three are about 2 to 2.5 psi (13.8 to 17.2 kPa). In column four, which is located at the northern free edge of the SSS, maximum seasonal snow pressure occurred at PCs 17 and 18 and was 3.85 psi (26.54 kPa).

4.4.3 Winter Season 2016 Snowpack Pressure Versus Time

Snow pressures recorded over the course of the 2016 winter season (January 1, 2016 through March 31, 2016) are shown plotted versus date for all twenty pressure cells in figures 30 through 34. The maximum recorded snow depth for the season was H_o = 62 inch (1.575 m), which occurred on January 30th. Row five of the PC array experienced zero pressure (within range of error) for the entire winter which is expected since the snow depth was just below the top crossbeam center. Similar to data recorded for the 2015 winter, figure 30 for column one illustrates that snow pressure intensity increases with downward distance from the snowpack top

surface. For all columns of PCs, the maximum pressures occurred around mid-height at PC rows three and four. In column one, maximum pressures were recorded during the first week in March with a maximum of 1.63 psi (11.24 kPa) and 1.53 psi (10.55 kPa) for rows three and four respectively. For column two, the highest recorded pressures occurred at the end of February and beginning of March with maximums of approximately 3 psi (20.68 kPa) near mid-height. In PC column three, maximum pressures at rows three and four were 2.8 psi (19.31 kPa) and 2.1 psi (14.48 kPa), respectively. These occurred in the month of March. In column four, at the northern free edge of the SSS, extreme pressure levels for the entire winter were recorded. Pressures of 3.4 psi (23.44 kPa), 5.2 psi (35.86 kPa), and 8 psi (55.16 kPa) were recorded at rows three, two, and one, respectively. The very high pressures recorded at rows two and three occurred in mid- to late March and these are the highest pressures recorded over the two winter seasons of data. The snow height during the period when these high pressures were observed was approximately 44 inch (1.118 m). This fact clearly illustrates that it is not snow depth alone that causes high slope-parallel pressures, but rather snowpack density and glide motion of the snow. Temperatures recorded near the bottom of the snowpack reached as high as 55 °F (12.8 °C) for the period of extreme pressures.

It is interesting to note that the pressures exerted on the SSS surface are very high only at column four, which is located at the northern edge of the SSS. Pressures one column inward at column three are at a maximum 3.5 psi (24.13 kPa) – why? The following explanation is given. At the very end of springtime when temperatures are well-above freezing, the snow releases completely from the ground surface and "wants" to move down the slope. The snow just north of the free edge of the SSS can in fact move while that at the edge of the SSS can't. It is postulated that the snowpack rotated as an entire block or mass and pivoted about the edge of the SSS, imparting very high pressures there while at the same time relieving pressures inwards as the block rotated. Essentially the phenomenon is akin to a block of material rotating about the corner of a table when the center of mass has been pushed past the edge of the table – gravity takes over and contact between the block is at only one finite point – the corner – as the block moves.

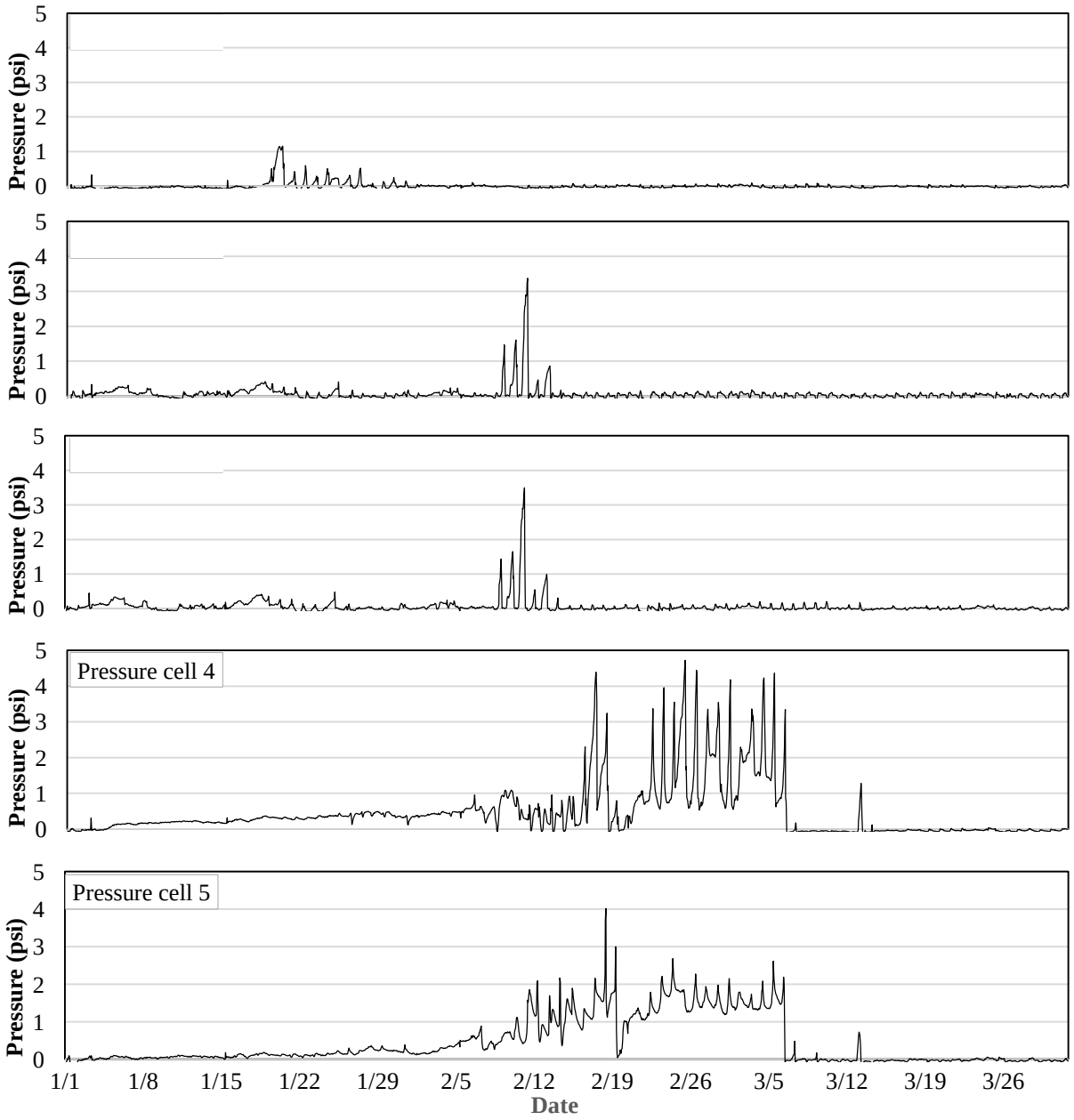

Figure 25 Snow pressures in column one for winter 2015

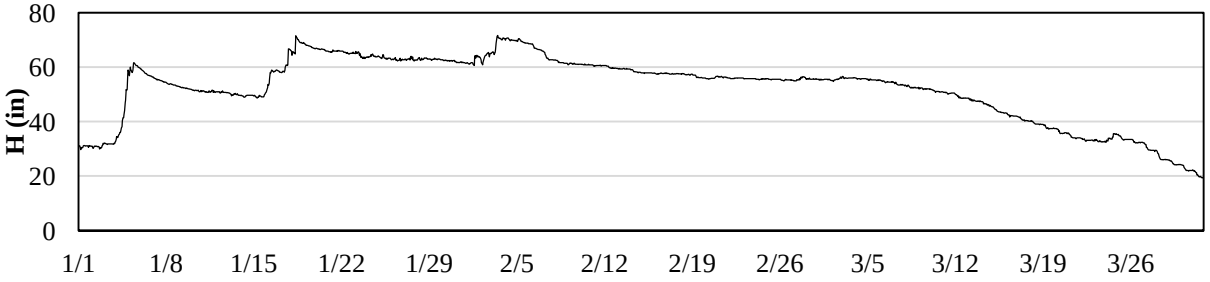

Figure 26 Snow height perpendicular to ground surface at column one for winter 2015

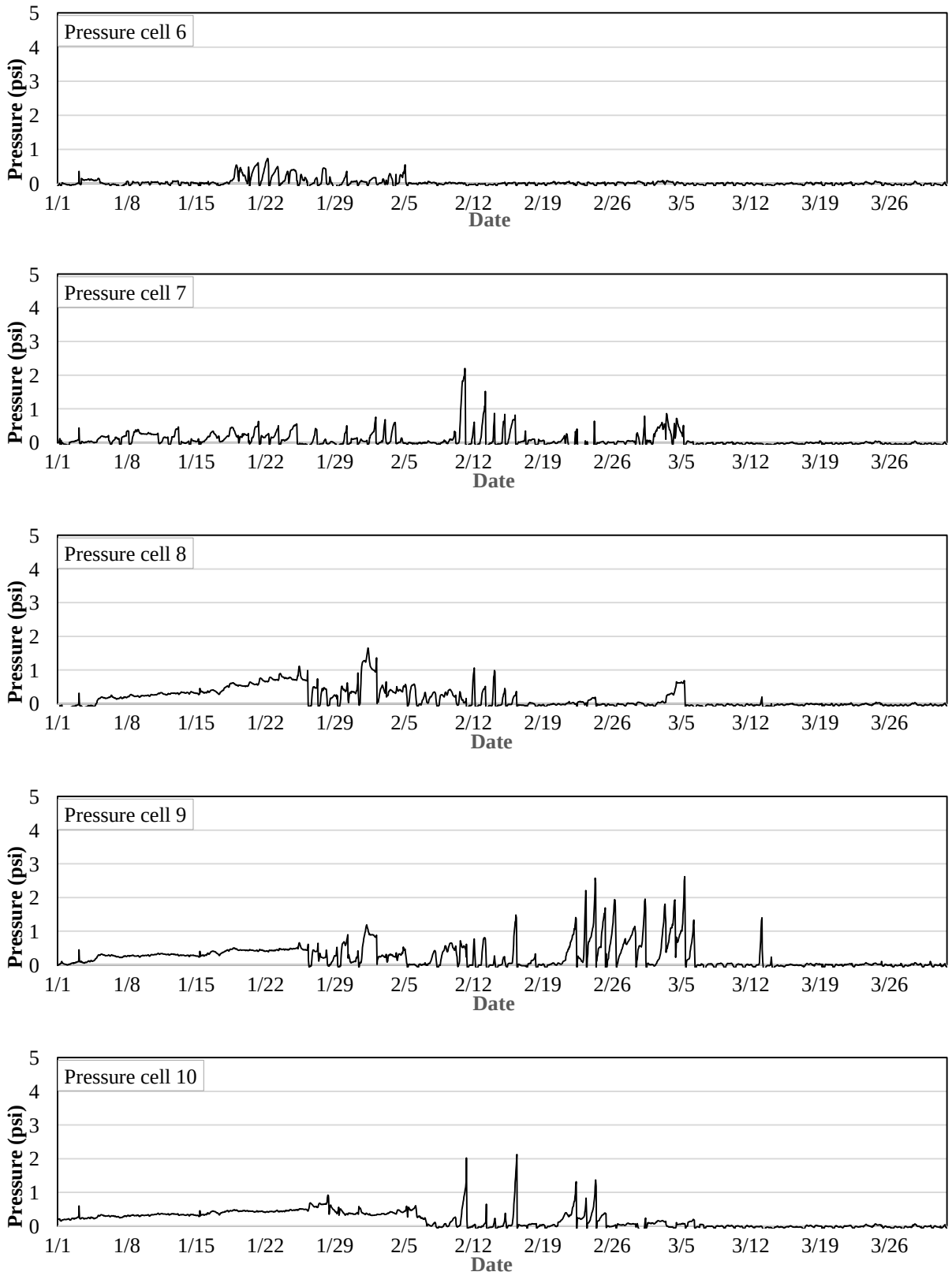

Figure 27 Snow pressures in column two for winter 2015

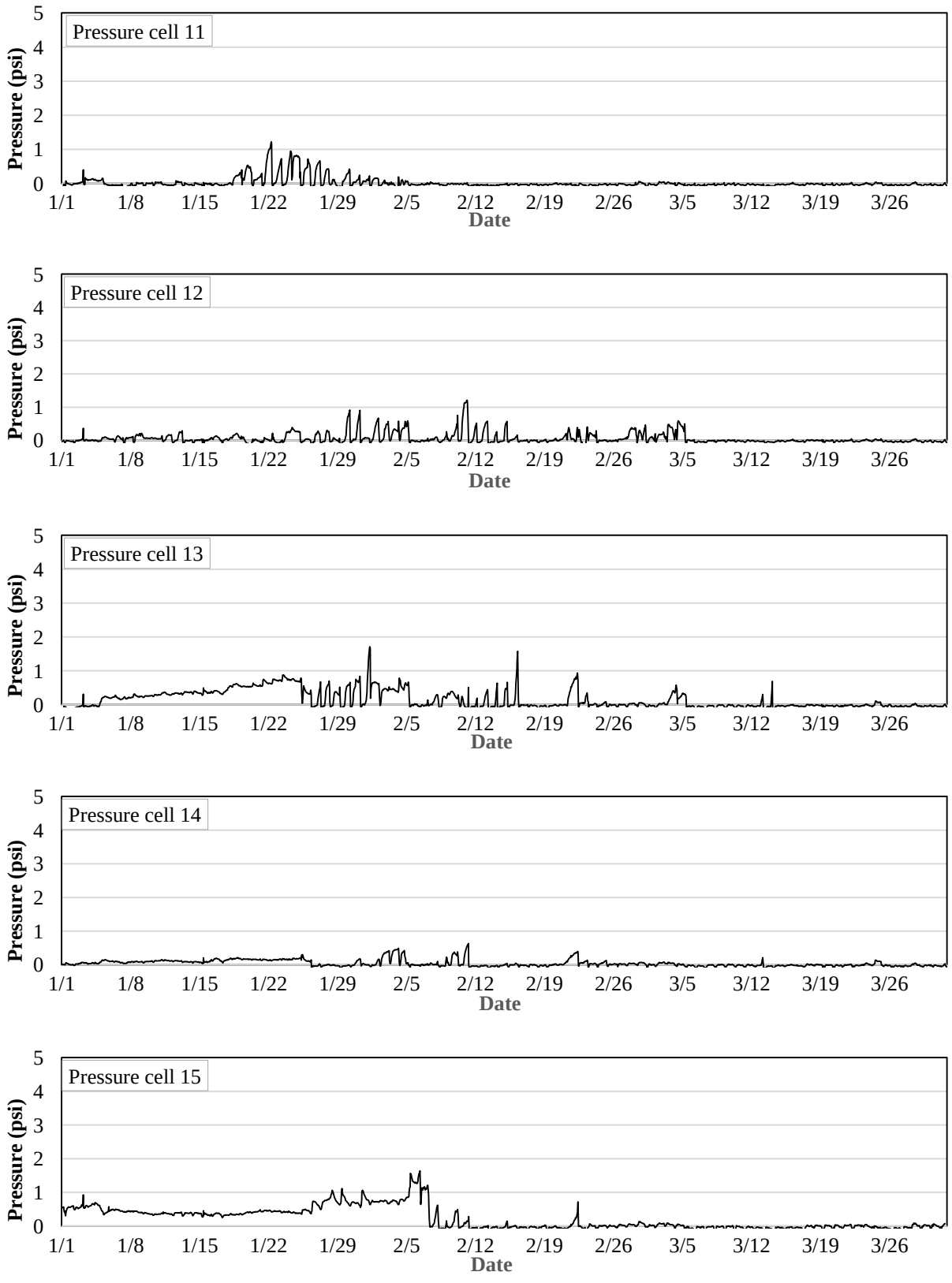

Figure 28 Snow pressures in column three for winter 2015

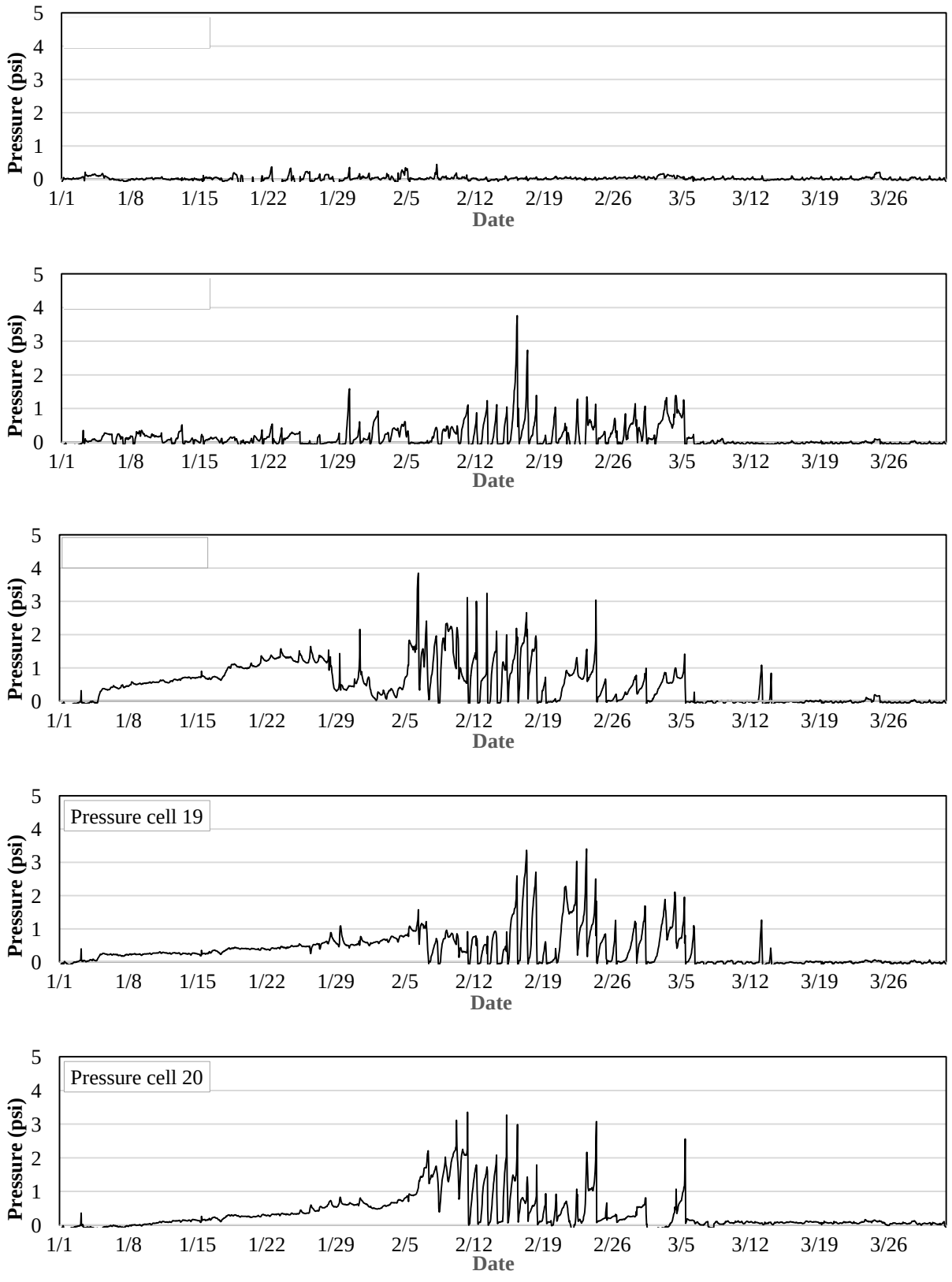

Figure 29 Snow pressures in column four for winter 2015

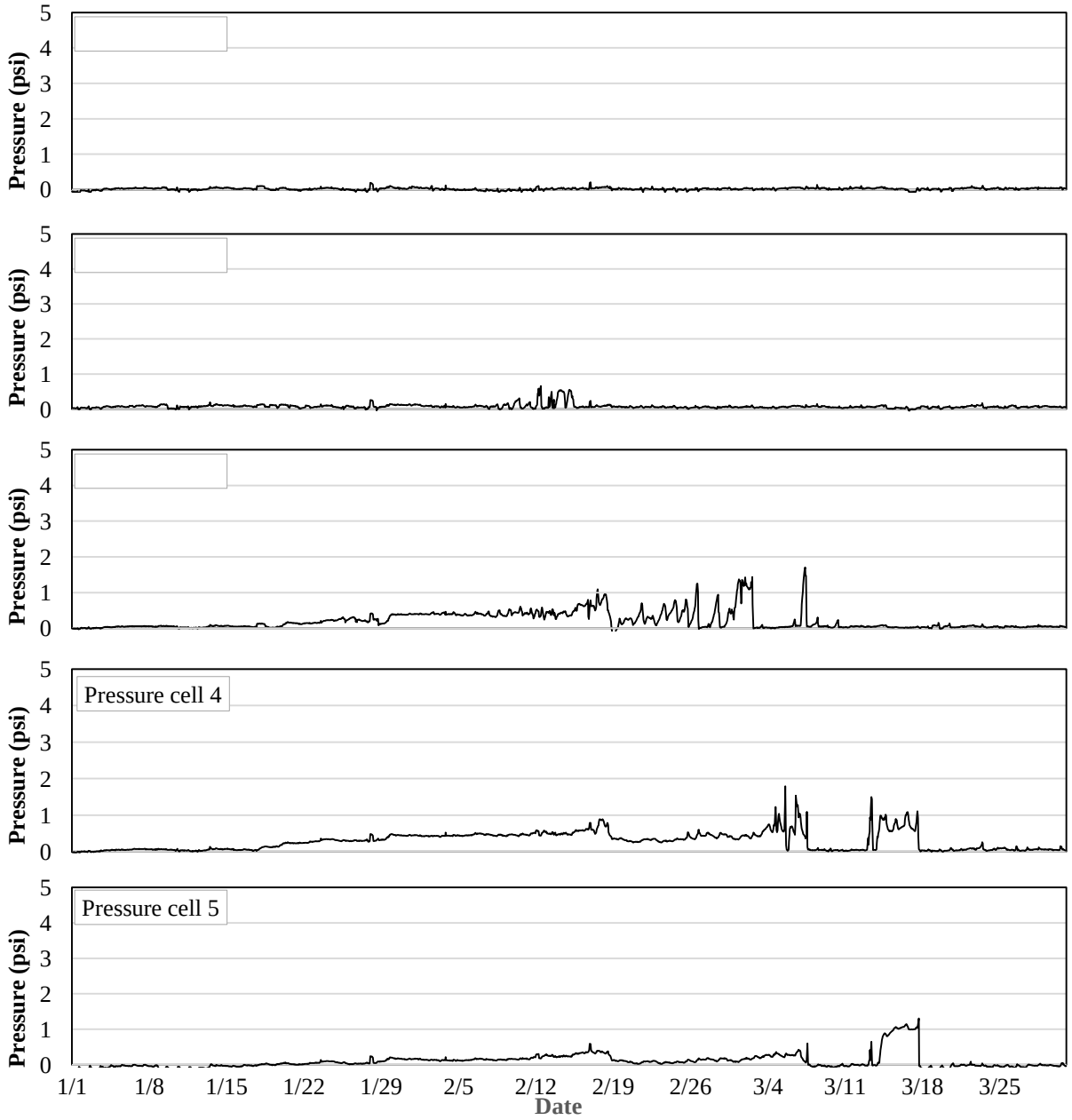

Figure 30 Snow pressures in column one for winter 2016

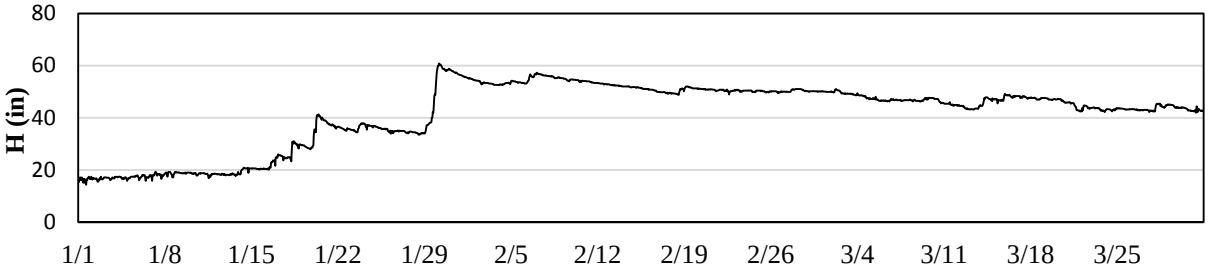

Figure 31 Snow height perpendicular to ground surface at column one for winter 2016

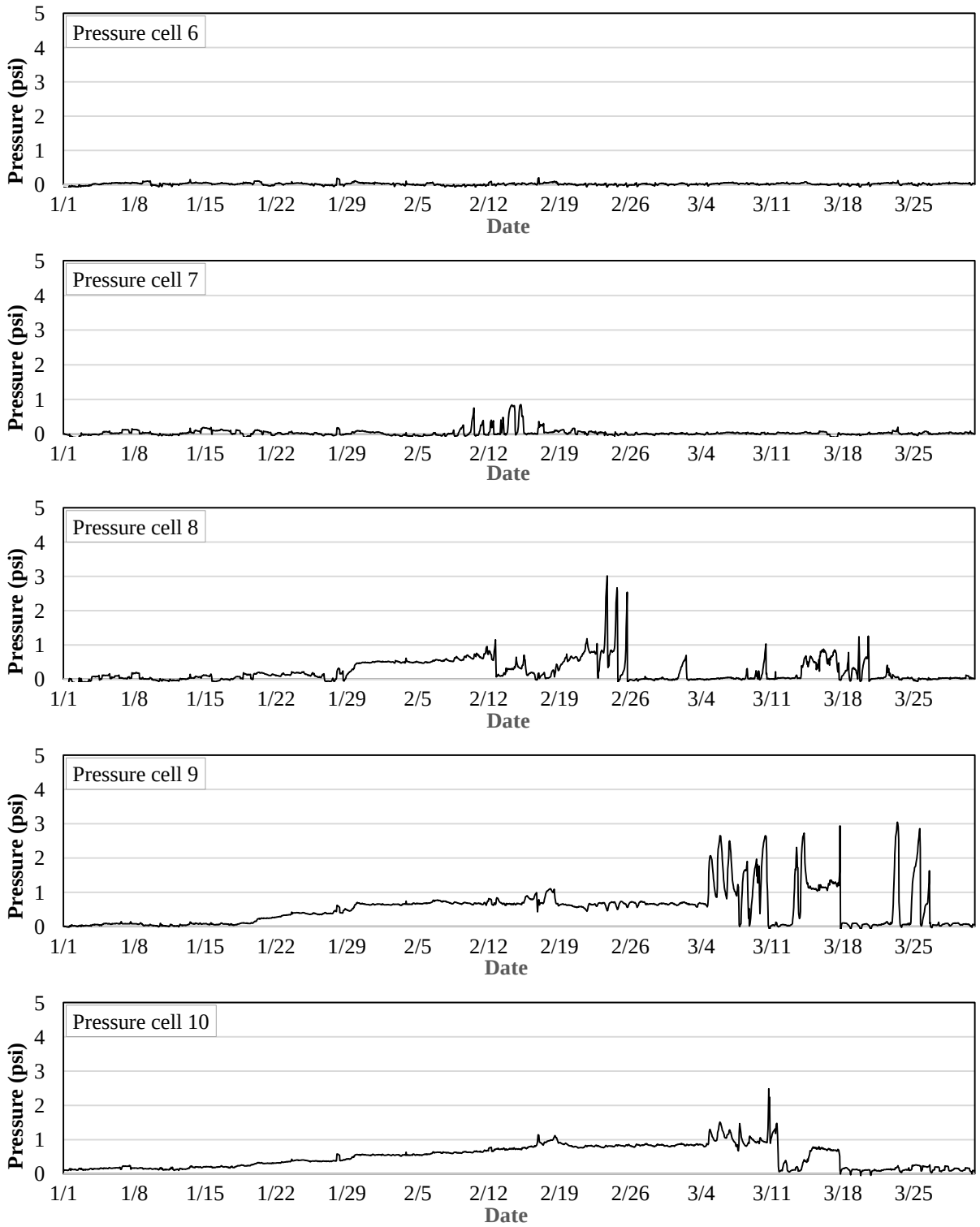

Figure 32 Snow pressures in column two for winter 2016

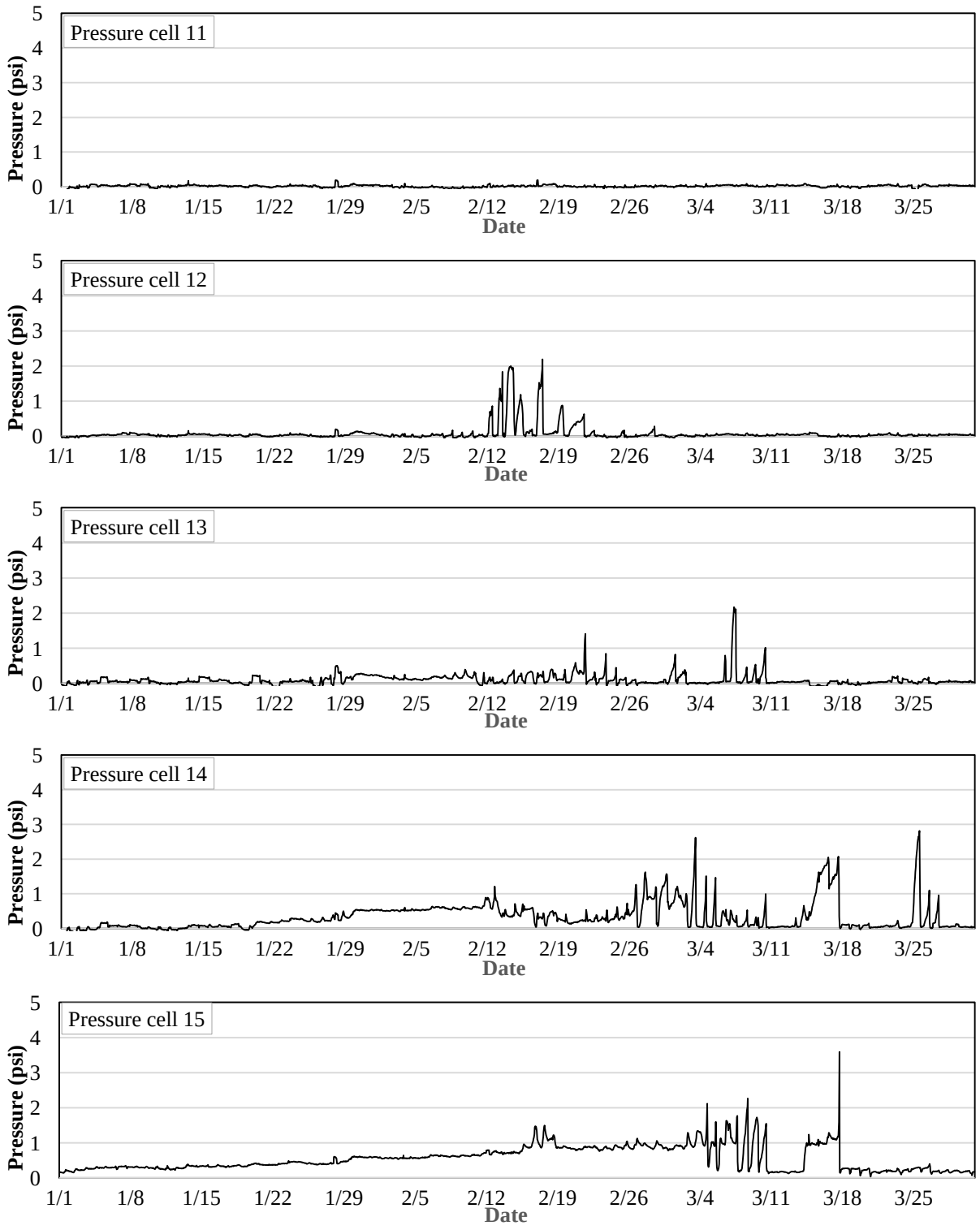

Figure 33 Snow pressures in column three for winter 2016

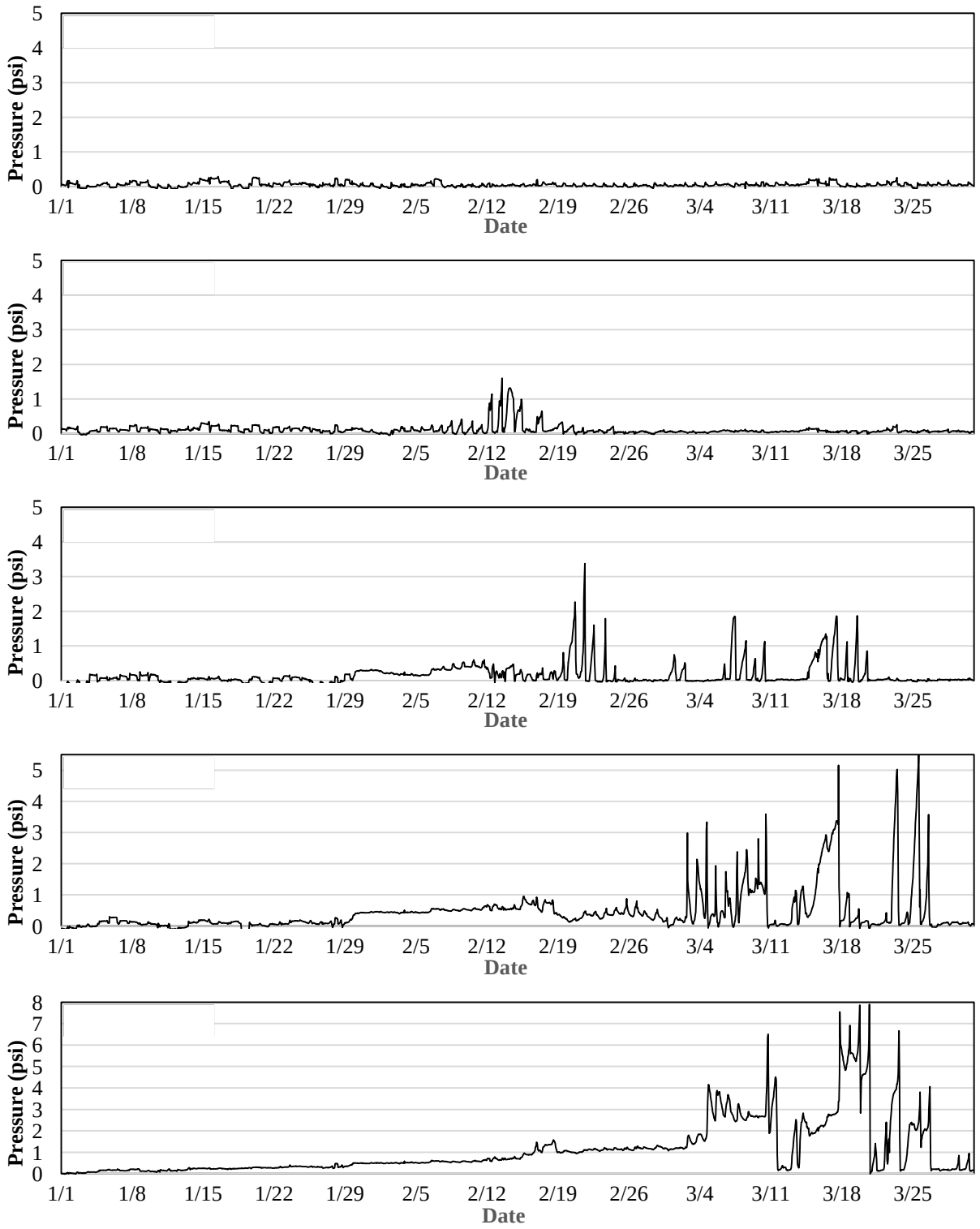

Figure 34 Snow pressures in column three for winter 2016 (* *Note different vertical axis scale for PC# 20*)

4.5 Comparison of Pressure Cell Results with Strain Gage Data

In order to assess the accuracy of the snow pressures determined using the barometric pressure and thermal adjustments described previously, a method was developed to compare SSS strut forces derived from both PC data and from strut vibrating wire strain gage data. First, the PC data was integrated over the full height and width of the snow supporting surface to obtain the total resultant snow force, R_{PC}. Values for the location or distance of this resultant force with respect to the foundation connection of the girder, d_R, were determined by static equilibrium principles (moment of the resultant about any point must equal the moment of the individual snow forces). Because the snowpack properties such as depth and density vary over the winter, this distance is not constant but rather is variable. To determine the strut axial compression force, C_{PC}, based on resultant snow force, a free-body diagram and static moment equilibrium are used, as shown in figure 35 below. If moments (force *x* perpendicular distance) are summed about Point *G*, at the girder connection to the foundation, only the strut force, C_{PC}, and the snow resultant force, R_{PC}, have non-zero moment arms. Note that the strut is assumed to have zero internal shear force because the top and bottom are assumed as pinned connections. Therefore, with no moments at top and bottom of the strut, there can be no shear force due to moment equilibrium of the strut. The distance between the axis of the strut and Point *G*, d_C, is found using information on the original project construction plans. The pertinent geometry is depicted in figure 36, and it can be seen that d_C = 38.5 inch x *cosine*(30°) = 33.34 inch (0.847 m). With reference to the free-body diagram of the SSS, summation of moments of all forces about Point *G* on the SSS yields the following equation based on moment static equilibrium:

— (14)

The strut axial compression force found in this fashion is that value that theoretically should be present internally within *both* struts combined since equilibrium of the SSS is by forces in two struts. Stated slightly differently, each strut would be expected to have one-half of C_{PC}, assuming the snow pressure was perfectly symmetric on the SSS (which it is not, but this is an assumption used as an overall check of snow pressure data).

Data recorded by the vibrating wire strain gages mounted to each strut provide normal (or axial) strains which can be used to calculate strut axial force by using Hooke's Law and the known strut cross-sectional area, A_{strut}, as given by equation 15 below:

(15)

In this equation, C_{VWSG} is the strut axial compression force, E_{steel} is the Modulus of Elasticity of steel taken as 29×10^6 psi (200 GPa) and ε is the normal strain from VWSG data. The total strut force providing equilibrium to the SSS under snow loads is that contained in both the north and south struts together, and thus force in the north side and south side struts are summed to determine C_{VWSG}.

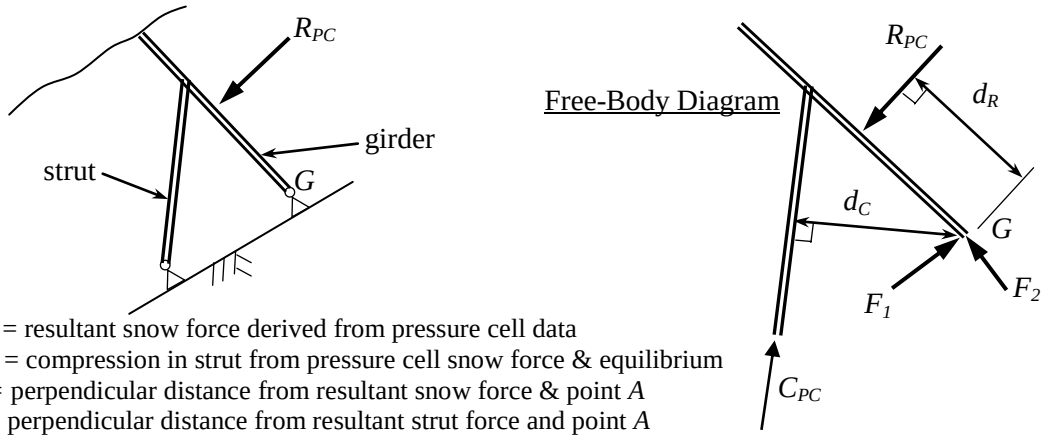

R_{PC} = resultant snow force derived from pressure cell data
C_{PC} = compression in strut from pressure cell snow force & equilibrium
d_R = perpendicular distance from resultant snow force & point *A*
d_C= perpendicular distance from resultant strut force and point *A*
G = A point at base of girder at bolted connection to foundation

Figure 35 SSS forces and free-body diagram used for equilibrium calculations

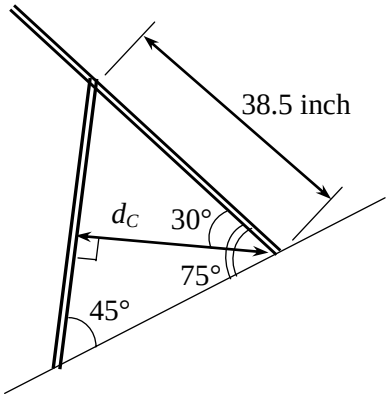

Figure 36 Geometry for moment arm of strut compression force, d_C

Values of strut compression force determined in the above detailed fashion for winter season 2015 are provided in table 3 below for four distinct dates over a two-month period. In February, the strut compression forces calculated from strain gage data are less than those predicted using PC data and equilibrium with ratios of 0.84 and 0.77 for February 1st and 15th, respectively. In March, the strain gage derived strut forces were greater than those calculated by PC data with ratios of 1.07 and 1.12 for March 1st and 15th, respectively. The average ratio of strut force by the two methods is 0.95 with a standard deviation of 0.17. Similar data for winter season 2016 is provided in table 4 for the same four distinct dates and the average ratio of strain gage derived strut axial force to that calculated based on snow pressure resultants and equilibrium is 0.86 with a standard deviation of 0.24. When both winter season ratios are used to calculate an average ratio, a mean ratio of 0.91 with standard deviation of 0.20 are obtained.

It is important to note that use of strain gages where thermal gradients are present is difficult because of time differences in heating and cooling of the strain gages and the objects to which they are attached. In the case of strain gages on the SSS struts, differences in temperatures of the VWSG and the steel strut to which it was mounted cause a thermal strain. Typically, the observed phenomenon in the data at mid- to late afternoon was tensile strains recorded by the vibrating wire strain gages even though the strut was in compression under the loading of the snowpack. This is due to the fact that the steel strut heats more quickly than the VWSG which is

insulated from the direct sun by a protective cover. Unfortunately, while this phenomenon takes place, the very same late-afternoon warming may be causing increased snow pressures due to release of snowpack from the ground. Because two phenomena are taking place simultaneously, it is difficult to determine how much additional compression strain might be caused by increased snow pressures due to glide and how much tensile strain is being induced by the time-lag in thermal heating of the VWSG. Because of this, when a net tensile strain was indicated by the VWSG at a given hourly recording point, only the data either several hours before or after the point was used to assess strut compression strain.

This comparison of strut force from two independent types of physical quantities is simply meant to provide for a check of the PC data for "reasonableness". Winter season 2015 exhibited slightly better correlation between strut forces than season 2016, but in total the data indicates that the pressure signals derived after making corrections for barometric pressure and temperature can be relied upon as being accurate. Finally, in contrasting the values of strut force calculated by VWSG and by equilibrium with integrated snow pressures, it is believed that the PC data is more reliable than the VWSG because of the above described difficulties with the VWSG.

Table 3 Comparison of pressure cell derived C_{PC} and strain gage derived C_{VWSG} SSS strut force, 2015

Date	North Strut		South Strut		C_{VWSG} (kip)	R_{PC} (kip)	d_R (in)	C_{PC} (kip)	C_{VWSG} / C_{PC}
	με	C_N (kip)	με	C_S (kip)					
2-1	-26.6	3.32	-24	2.99	6.31	7.66	32.66	7.46	0.85
2-15	-39.0	4.86	-29	3.62	8.50	12.0	30.7	11.0	0.77
3-1	-39.7	4.94	-34.5	4.30	9.24	11.3	25.54	8.66	1.07
3-15	-23.5	2.93	-32.5	-4.05	6.98	7.91	26.16	6.21	1.12

Table 4 Comparison of pressure cell derived C_{PC} and strain gage derived C_{VWSG} SSS strut force, 2016

Date	North Strut		South Strut		C_{VWSG} (kip)	R_{PC} (kip)	d_R (in)	C_{PC} (kip)	C_{VWSG} / C_{PC}
	με	C_N (kip)	με	C_S (kip)					
2-1	-8.0	1.0	-10.0	1.24	2.24	2.42	25.4	1.85	1.21
2-15	-21.0	2.62	-17.0	2.10	4.72	7.25	31.0	6.74	0.70
3-1	-30.0	3.74	-20	2.50	6.24	10.80	28.4	9.2	0.68
3-15	-23	2.87	-21.5	2.68	5.55	11.87	18.6	6.60	0.84

4.6 Pressure Variation Across SSS Width

Analysis of the pressure variation across the width dimension of the SSS was performed to yield information about SSS end-effect pressures for comparison with the Swiss Guide end-effect provisions. Because the attribute of interest is how snow pressures vary in a lateral dimension from the middle of a SSS to the free edge where there is no adjacent SSS, pressures were plotted grouped by row number and against the horizontal distance from the southernmost free edge of the instrumented SSS. As stated previously, end-effects are expected to be greatest during springtime when glide motions are the largest due to thawing of the snowpack-to-ground interface under warming conditions. Graphs of pressure across width were compiled by two week periods to investigate this. For the instrumented SSS, the north free edge has no adjacent

SSS (next SSS on the same contour line is approximately 30 ft (9.14 m) to the north) and thus pressure cell data from columns four and five and within each row were used to calculate experimental values of end-effect factor, f_R by equation (16):

(16)

4.6.1 Winter Season 2015

For the first two week period, pressures are well-below the seasonal maximums and pressures in rows two, four, and five are similar for columns three and four (figure 37). Row three does exhibit increasing pressure going from the interior of the frame (columns two and three) to the exterior column of pressure cells – column four. Ratios of column four to column three pressures were calculated for all dates in the experimental data set and these correspond to $1 + f_R$ since the end-effect factor is the additional pressure to be added to the basic pressure without end-effects. For the period from January 1st to January 15th, 2015, the average end-effect factor was $f_R = 0.5$. For the period between the 1st and 15th of February, rows one through three exhibit an increase in snow pressure at the end-effect region of column four (figure 38). For this period, the average end-effect factor was $f_R = 1.5$. In mid-February, daytime ambient temperatures began rising significantly above freezing – on February 17th the daytime high temperature reached 55 °F (12.8 °C). Thus, release of the snowpack from the ground and high glide rates would be present. This is reflected in the pressure versus width graphs for the period between February 15th and March 1st, 2015 where every row except row five exhibits a marked increase in snow pressure at column four, or the free edge of the SSS (figure 39). Row five doesn't exhibit the increase in pressure within the end-effect region because the snow cover height was below that row of pressure cells and the pressure signals were essentially zero. Also notable is that end-effect pressures are at or near their seasonal maximums, and this correlates well with snow pressure theory – highest pressure effect comes from the glide phenomenon, which is biggest in the spring. For the period from February 15th to March 1st, 2015, the average end-effect factor was $f_R = 3.9$. Finally, from March 1st to the 15th, pressures within column four are significantly elevated compared to those in the adjacent column three with an average end-effect factor of $f_R = 4.9$ (see figure 40).

To assess the most appropriate date range for determination of an average experimental end-effect factor, snowpack temperature near the snow – to – ground interface was plotted using temperature recordings from PC#10. Figure 41 illustrates the snowpack temperatures were above freezing daily starting at about the second week in February. Thus, it can be assumed that the snow cover released from the ground mostly daily from mid-February until the end of the snow season. Because of this and the fact that the end-effect phenomenon will be greatest when glide motion is the greatest, an average experimental end-effect factor for mid-February through mid-March was calculated as was $f_R = 0.5 \times (3.9 + 4.9) = 4.4$. To further explore the temperature dependence of end-effects, the end-effect factors calculated for each two-week period are shown graphed as a function of maximum daily snow cover temperature in figure 42. For the 2015 winter season, it is clearly evident that the highest end-effects occur only when the snowpack temperature rises well-above freezing, i.e. 32 °F (0 °C). The average end-effect factor when the maximum snowpack temperature remained below freezing is $f_R = 0.4$, while the same for periods with temperature above 32 °F (0 °C) is $f_R = 3.5$.

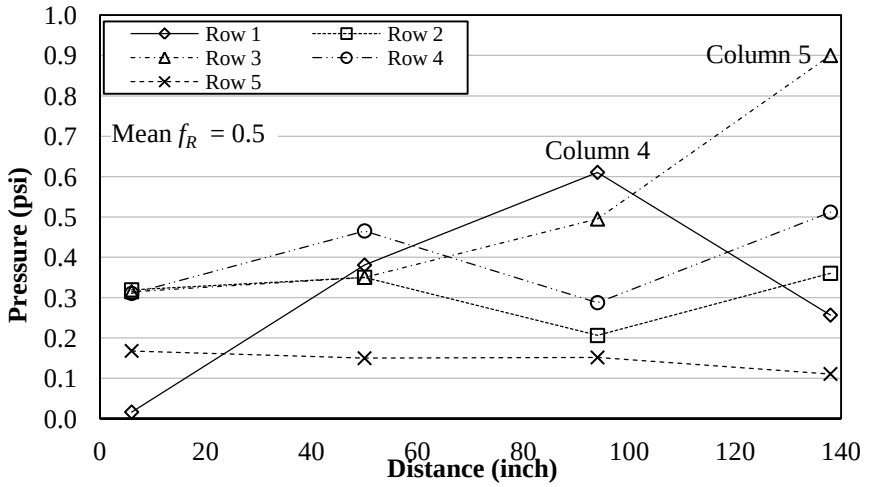

Figure 37 Snow pressure distribution across width for January 1st to January 15th, 2015

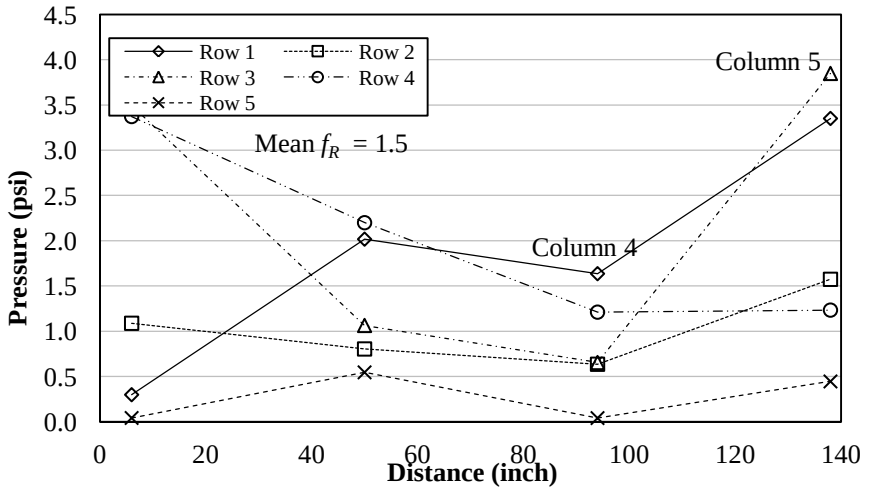

Figure 38 Snow pressure distribution across width for February 1st to February 15th, 2015

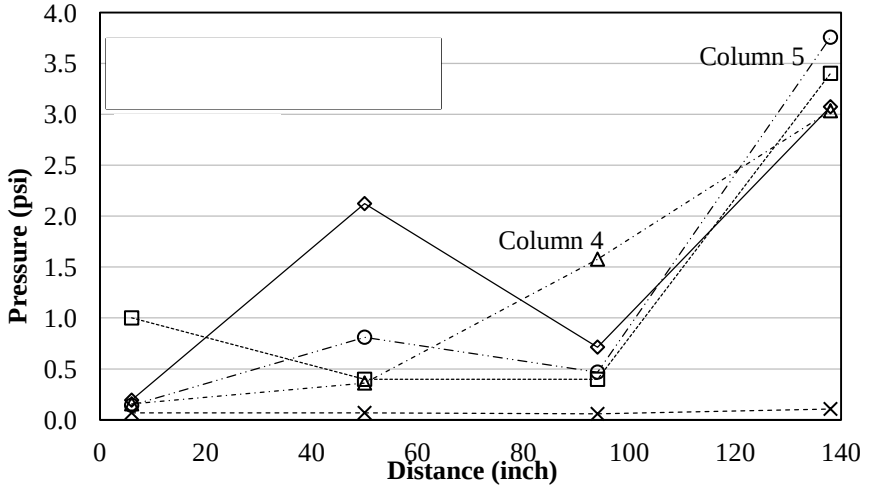

Figure 39 Snow Pressure distribution across width for February 15th to March 1st, 2015

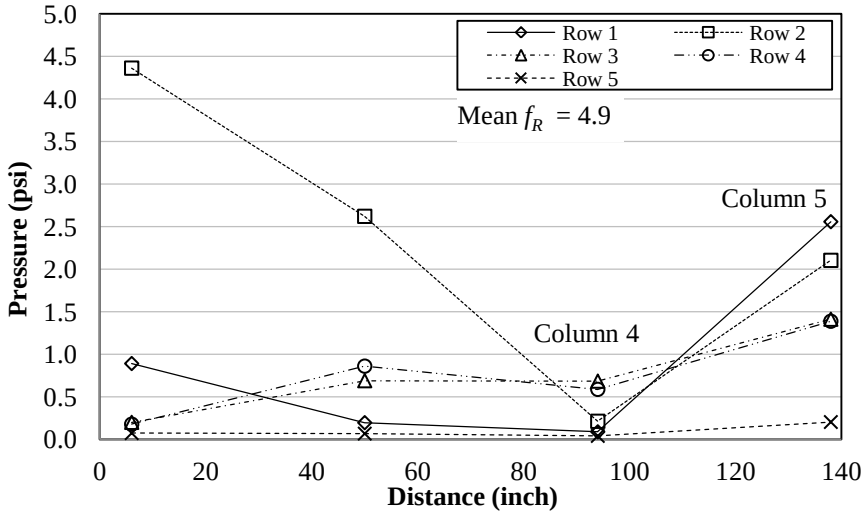

Figure 40 Snow pressure distribution across width for March 1st to March 15th, 2015

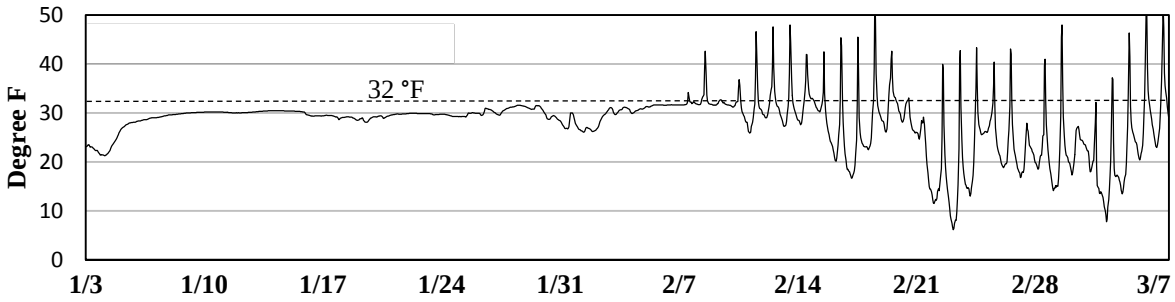

Figure 41 Snow cover temperature at row one of SSS for winter 2015

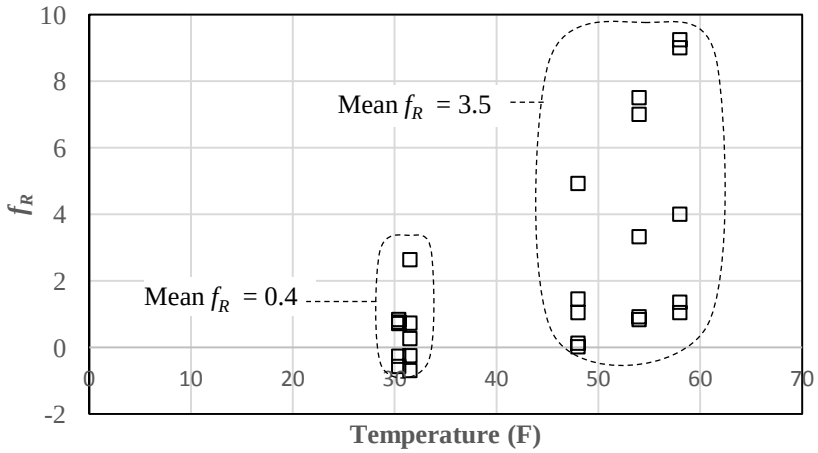

Figure 42 Temperature dependence of end-effect factor, f_R, 2015

The final illustration of pressure versus SSS width for the 2015 season is shown in figure 43, which is absolute maximum pressures recorded over the entire winter season irrespective of time (all previous pressure versus width graphs were based on bi-weekly data sets). While the pressure versus width data plotted in this fashion is less meaningful with respect to end-effect

factor numeric values, it shows the general trend of increased snow pressure at the free edges of the SSS as compared to those occurring near the middle of the SSS and away from the free edges. Clearly it is evident that snow pressures in the end-effect region are at least double those occurring near the interior and for which the theoretical snow pressure equations have been developed.

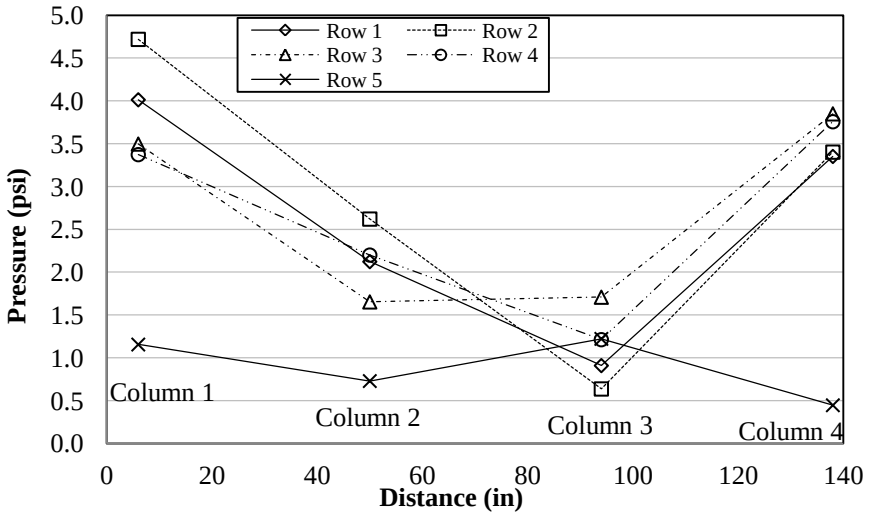

Figure 43 Snow pressure distribution across width direction of SSS for 2014-2015 Season

4.6.2 Winter Season 2016

For the first two week period of January 1st to January 15th, 2016, pressures are well-below the seasonal maximums and pressures are greater in the end-effect region (column four) except for row one (figure 44). The maximum snowpack temperature in row one for this period was 31 °F (-0.6 °C). and the average end-effect factor was f_R = 5.9. It is noted however that the pressures overall are extremely small – 0.35 psi (-2.41 kPa) as a maximum – and thus this end-effect factor should not really be extrapolated to apply to the maximum seasonal pressures that occur along with high snow temperatures and glide rates. For the period between the 1st and 15th of February, end-effect region snow pressures are not on average significantly greater than those near the middle of the SSS, and the maximum daily snowpack temperature at row one was 31 °F (-0.6 °C) (figure 45). For this period, the average end-effect factor was f_R = 0.6. For the period of February 15th to March 1st, the maximum daily snowpack temperature was 31 °F (-0.6 °C) and only rows two and three exhibit a marked increase in pressure at the end-effect region (see figure 46). For this period, the average end-effect factor was f_R = 0.1. For the final period of March 1st to March 15th, the snowpack height was below rows four and five and thus snow pressures were essentially zero for this period, and the maximum daily snowpack temperature was above freezing at 44 °F (6.7 °C) (figure 47). Row one shows the biggest end-effect pressure increase, and excluding rows four and five because of lack of snow, the average end-effect factor was f_R = 0.70.

Generally speaking, the maximum snowpack temperature near the ground surface over the winter season 2016 remained below the freezing mark. This is reflected in the small end-effect factors, which agrees with theory since highest end-effects typically only occur when the snowpack temperatures rise well-above freezing. End-effects factors for the two-week periods

are shown plotted against maximum daily snowpack temperature in figure 48, with data from the first two-week period of January 1st to 15th excluded based on the reasoning given previously. The average end-effect factor when the maximum snowpack temperature remained below freezing is f_R = 0.3, while the same for periods with temperature above freezing is f_R = 0.7.

The final illustration of pressure versus SSS width for the 2016 season is shown in figure 49, which is absolute maximum pressures that occurred over the entire winter season irrespective of time. Similar to the same figure for 2015, the data clearly indicate a positive correlation between higher snow pressures occurring in the end-effect region. Similar to winter 2015 data, the 2016 data indicate that end-effect pressures are at least two times greater than those occurring near the middle of a SSS.

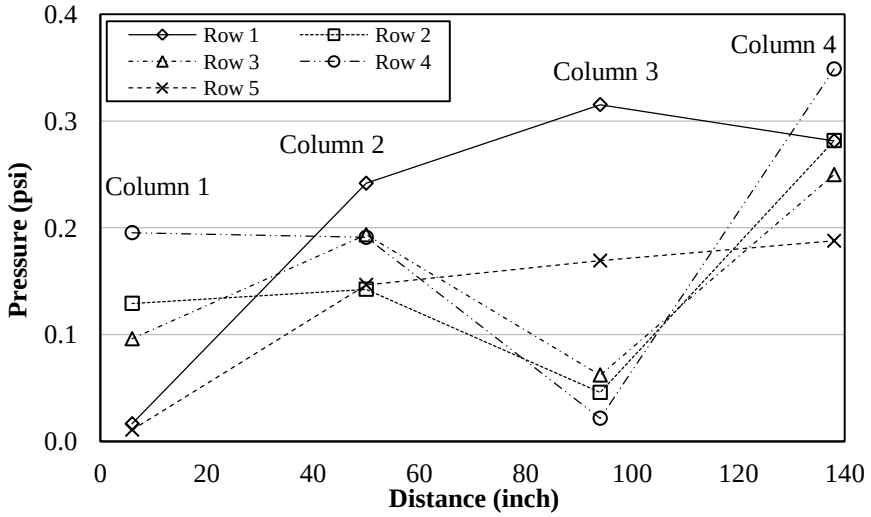

Figure 44 Snow pressure distribution across width for January 1st to January 15th, 2016

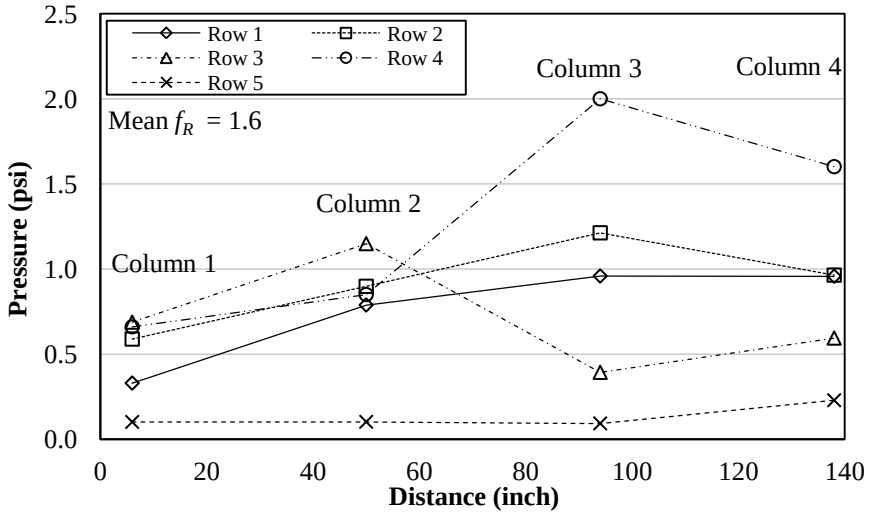

Figure 45 Snow pressure distribution across width for February 1st to February 15th, 2016

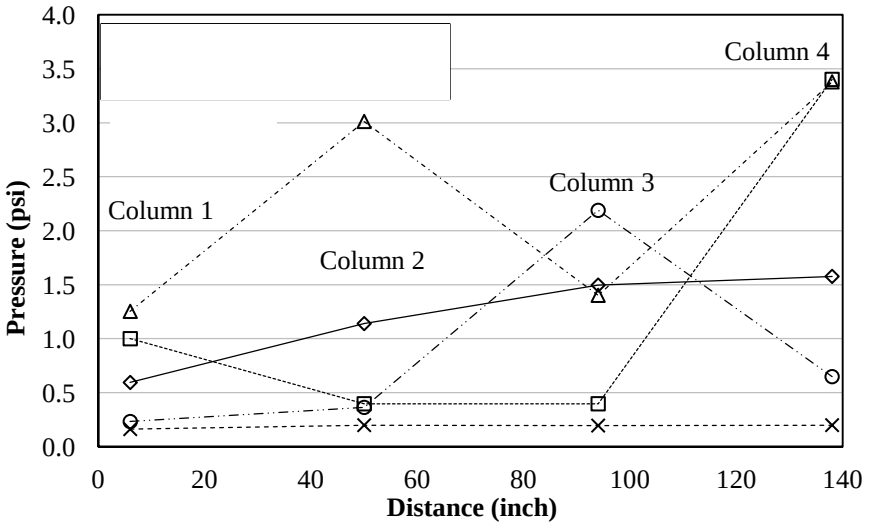

Figure 46 Snow pressure distribution across width for February 15th to March 1st, 2015

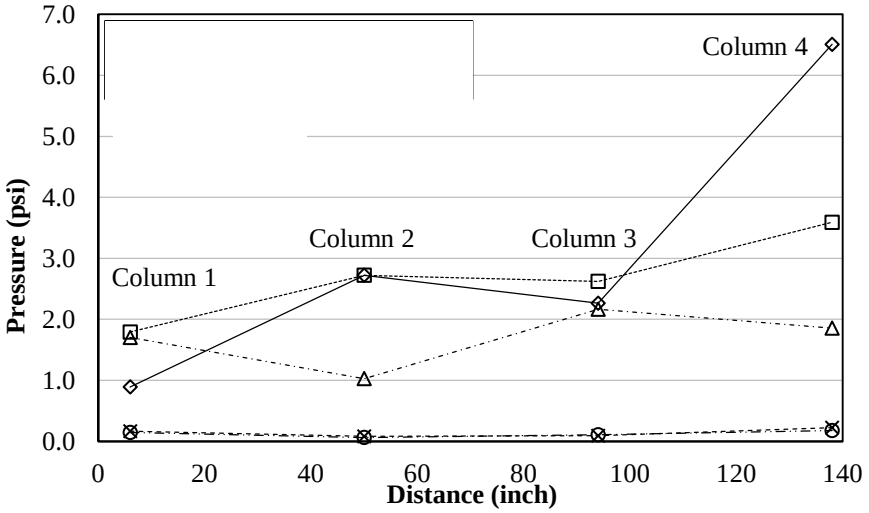

Figure 47 Snow pressure distribution across width for March 1st to March 15th, 2015

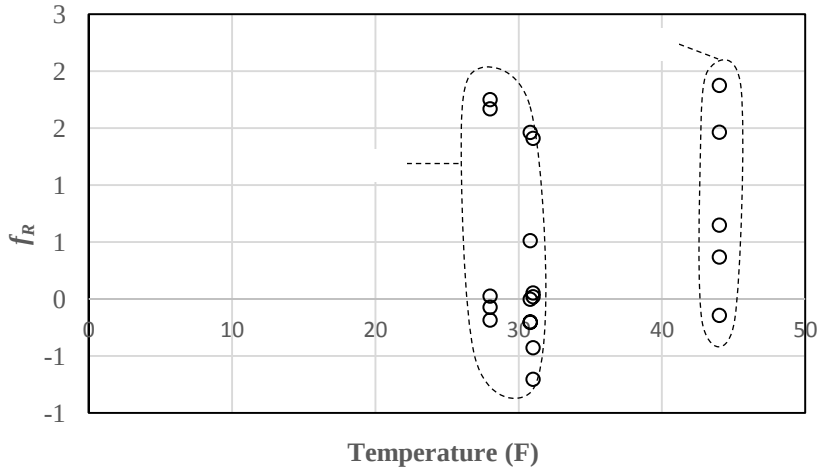

Figure 48 Temperature dependence of end-effect factor, f_R, 2016

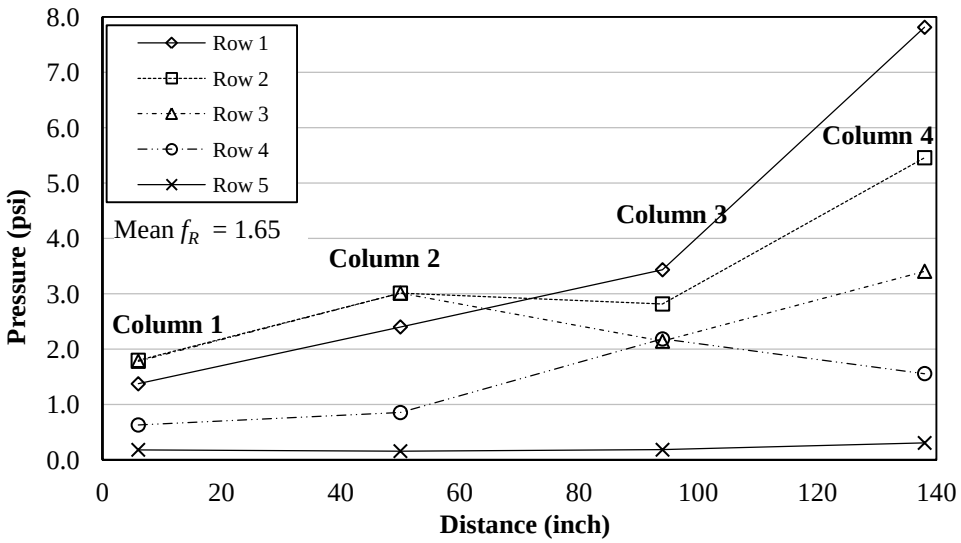

Figure 49 Snow pressure distribution across width direction of SSS for 2016 Season

4.7 Snow Pressure Resultants and Average Pressures

In order to calculate an average uniform pressure acting on the SSS, the total resultant snow force must be determined, and calculation of total resultant snow force acting on SSS follows from fundamental statics and mechanics: integration of pressure over surface area. That is, the three-dimensional pressure distribution recorded by all twenty PCs is integrated over the area of the grate surface of the SSS. However, in order to determine the average snow pressure across different zones of the SSS (i.e. end-effect zone or interior region away from end-effect zone), snow force resultants for the four different columns defined in figure 8 are needed. This is accomplished by integration of the pressure profile over the height of the SSS and over a width that the pressure profile is assumed to act. Figure 50 illustrates the individual resultant snow forces, S_i, which act over height regions, h_i, and that are located at distances, d_i, from the reference datum which is located at the center of the top row of pressure cells (row 5). For each snow force S_i, the pressure recordings at locations *"i"* and *"i+1"* (i.e. pressure cells in two adjacent rows and the same column) are averaged and then multiplied by height h_i and width w_k.

The heights in this procedure are the distances between the centers of pressure cells in adjacent rows, which is a constant 14 inch (0.356 m) between rows two, three, four, and five, and 13 inch (0.330 m) between rows one and two (refer to figure 9 which depicts dimensions of SSS from original construction plans). The lowest height, h_1, corresponds to one-half the distance between row one and the ground surface (i.e. tributary height), and this is h_1 = 4.5 inch (0.114 m).

The widths used in the integration of pressure over SSS area are based on the tributary widths or distances between adjacent columns of pressure cells. The tributary width of pressure for column one is one-half the distance to the adjacent column, which is column two. From figure 9, this distance is (50 – 6) x 0.5 = 22 inch (0.559 m). The total width for column one is 6 + 22 = 28 inch (0.711 m). Column four has the same geometry and hence same tributary width as column one. Interior columns two and three have tributary widths for pressure integration of 44 inch (1.12 m).

Snow force resultants obtained by the above described process are forces perpendicular to the SSS grate surface, which itself is not perpendicular to the ground surface as shown in figure 1.

Because the analytical snow pressure models provide snow pressure components parallel to the slope, the experimental force resultants are converted to slope-parallel components as shown in figure 51. Based on the geometry, the slope-parallel snow force resultant components are given by equation (17) as:

(17)

Snow pressure resultant forces for both 2015 and 2016 winters are provided in tables 5 and 7. Tables 6 and 8 provide resultant forces that are parallel to the ground slope for each column, and also a total resultant force, S_R, acting on the entire SSS for winters 2015 and 2016, respectively. Finally, average uniform snow pressures acting for each column of the SSS were calculated by dividing the resultant slope-parallel snow force by the snow height, H_o, present for that period, and these are given in tables 9 and 10. These average experimental snow pressures are those to be compared with the average snow pressures predicted by the analytical expressions in the Swiss Guide and by McClung, and this comparison is provided in chapter 6 of this report.

The height to the resultant snow force, h_N, was also calculated for the two winter data sets (see figure 51), and the ratio between these heights and the snowpack height are tabulated in tables 5 and 7. The height to the resultant snow force is a critical design parameter for overall SSS stability since by equilibrium (see figure 35) it directly influences the magnitude of the foundation reactions and axial force in the strut and girder. As this height to resultant increases, so too would the foundation reactions. The average height to snow force resultant from the ground surface, expressed as a fraction of snowpack height, H_o, was 0.55 with a standard deviation of 0.03 for winter 2015. For the 2016 winter data set, the average was 0.56 with a standard deviation of 0.07. The average for both winter seasons is 0.56 with 0.05 standard deviation.

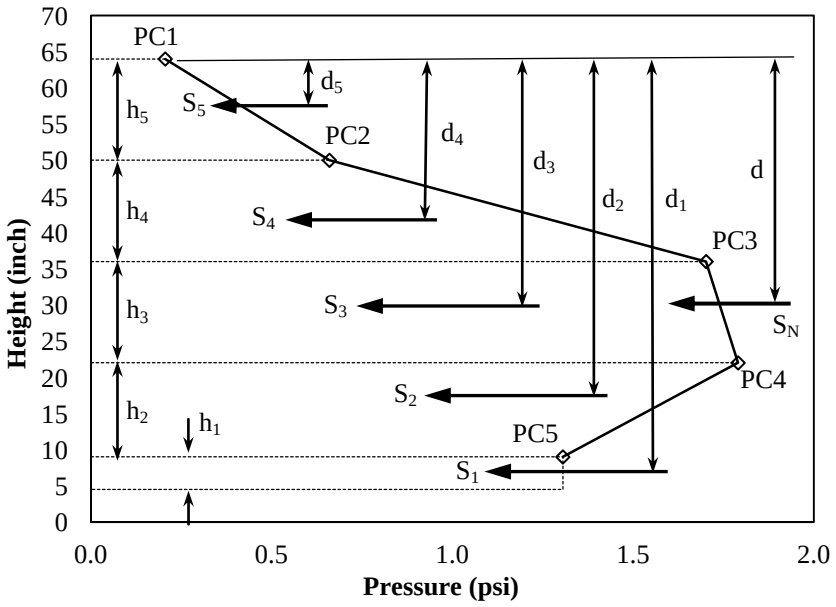

Figure 50 Integration scheme of pressure on SSS for snow force resultant and resultant location

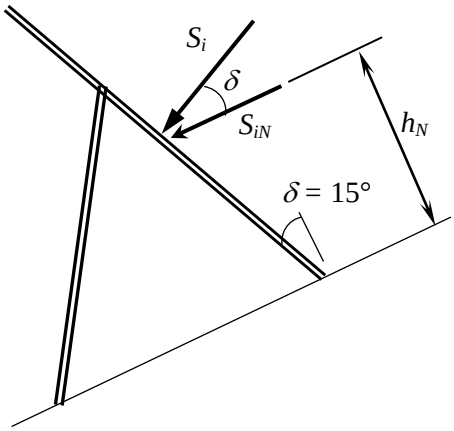

Figure 51 Snow pressure resultant and slope-parallel force component

Table 5 Resultant snow forces by integration over SSS surface for winter 2015 [lb]

Date	**Column 1**	**Column 2**	**Column 3**	**Column 4**	**Total, S_R**	**h_N / H_o**
1/15	438	1316	940	677	3371	0.51
2/1	557	2490	2881	1736	7664	0.57
2/15	2765	3965	2544	3179	12452	0.55
3/1	1781	3446	1977	4103	11306	0.51
3/15	1761	2859	1057	2233	7910	0.57

Table 6 Resultant slope-parallel snow force by integration on SSS surface for winter 2015 [lb]

Date	**Column 1**	**Column 2**	**Column 3**	**Column 4**	**Total, S_R**
1/15	423	1271	908	654	3256
2/1	538	2405	2783	1677	7403
2/15	2670	3829	2457	3070	12028
3/1	1720	3328	1910	3963	10921
3/15	1701	2762	1021	2157	7640

Table 7 Resultant snow forces by integration over SSS surface for winter 2016 [lb]

Date	**Column 1**	**Column 2**	**Column 3**	**Column 4**	**Total, S_R**	**h_N / H_o**
1/15	158	447	487	182	1274	0.55
2/1	445	784	740	435	2403	0.53
2/15	747	2359	2913	1329	7348	0.65
3/1	967	3625	4286	2078	10956	0.62
3/15	1102	3545	4022	3127	11795	0.48

Table 8 Resultant slope-parallel snow force by integration on SSS surface for winter 2016 [lb]

Date	Column 1	Column 2	Column 3	Column 4	Total, S_R
1/15	152	432	470	176	1231
2/1	430	757	715	420	2322
2/15	721	2278	2814	1284	7098
3/1	934	3501	4140	2007	10583
3/15	1064	3424	3885	3020	11393

Table 9 Average snow pressures by column acting on SSS for winter 2015 [lb/ft^2]

Date	Column 1	Column 2	Column 3	Column 4
1/15	0.32	0.48	0.34	0.50
2/1	0.39	0.86	1.0	1.2
2/15	1.8	1.3	0.83	2.1
3/1	1.3	1.2	0.71	2.9
3/15	1.3	1.0	0.38	1.6

Table 10 Average snow pressures by column acting on SSS for winter 2016 [lb/ft^2]

Date	Column 1	Column 2	Column 3	Column 4
1/15	0.16	0.23	0.24	0.18
2/1	0.33	0.29	0.28	0.32
2/15	0.57	0.90	1.1	1.0
3/1	0.77	1.4	1.7	1.7
3/15	0.99	1.6	1.8	2.8

4.8 Average Versus Maximum Snow Pressures

Of particular interest for design of individual components such as horizontal crossbeams is the relationship between the maximum snow pressure that occurs along the snow height versus the average or uniform value. Recall from figure 3 given previously that a uniform pressure distribution is applied to a SSS for design purposes even though it is known that actual pressures vary within the snowpack thickness. While the average snow pressure determined as described in the previous section of this report will give the same total resultant snow force as the actual pressure distribution (from which the average was derived), localized higher snow pressures can be expected to act near mid-height of the structure. To illustrate this, actual snow pressures acting along the height of the snow cover for a specific column were plotted on a horizontal axis against height, H_o, on the vertical axis. Figure 52 below provides the depth variation of pressures measured in PC column one over the course of winter 2016. It is very clear that snow pressures are anything but uniform, and resemble the increasing pressure with depth and then tapering back to lower pressure near the ground surface that was described in chapter two. The figure also indicates that the largest snow pressures occur in the springtime when glide motion is expected to be the highest. For the March 14th bi-weekly period, the snow pressures are the highest for the

season even though the snowpack height had begun to decrease significantly by that time (see figure 26). To illustrate the relationship between the average (uniform) pressure and the maximum pressure, the average uniform pressure for column four for the February 28th, 2015 data set (see table 9) is plotted with the actual pressure along the height of SSS in figure 53. The maximum snow pressure within column four occurred at PC#17 and was σ_{Max} = 3.8 psi (26.2 kPa) while the average (uniform) pressure was σ_{Ave} = 2.9 psi (20.0 kPa). The maximum pressure was therefore 31 percent greater than the uniform pressure distribution. Figure 54 illustrates a similar comparison but for column one for the February 15th, 2016 period (see table 10). The maximum pressure within column one for this bi-weekly period occurred at PC#3 and was σ_{Max} = 0.69 psi (4.76 kPa) while the average pressure was σ_{Ave} = 0.57 psi (3.93 kPa). This represents a 21 percent higher actual pressure than the average pressure.

Ratios of maximum pressure within each column to the average pressure for that column were calculated for the bi-weekly periods of the data in tables 9 and 10. These ratios are given in tables 11 and 12 below. For winter 2015 data, the mean ratio of maximum-to-average snow pressure for all columns and all bi-weekly periods was 1.90 with a standard deviation of 0.62 (n=24), while for winter 2016 the mean was 1.65 with a 0.28 standard deviation (n=20). When the data for both winters is combined, the mean is 1.8 with a standard deviation of 0.50. The significance of the above is that localized snow pressures can be as high, on average, as 1.8 times the average or uniform pressure assumed as a simplification for design. It should be stated that this "simplification" is necessary because no analytical models have yet been developed to predict slope-parallel snow pressures as a function of height within the snow cover. It is also of interest to note that the maximum snow pressures typically (but not always) occurred at PCs mounted in rows two, three, and four. These rows are those crossbeams located within the middle 50 percent of SSS height.

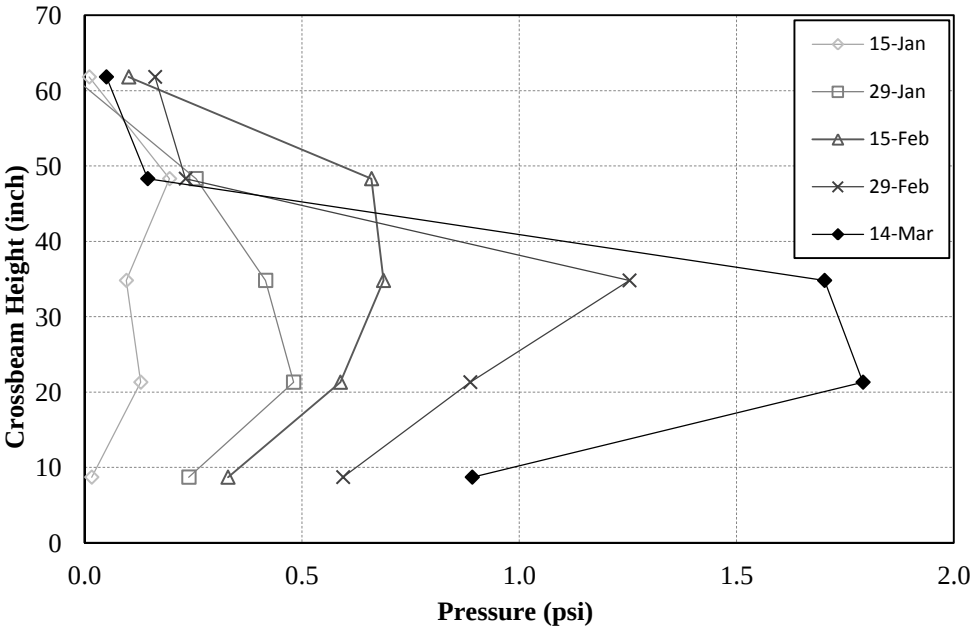

Figure 52 Bi-Weekly snow pressure variation along height of SSS within PC column three for winter 2016

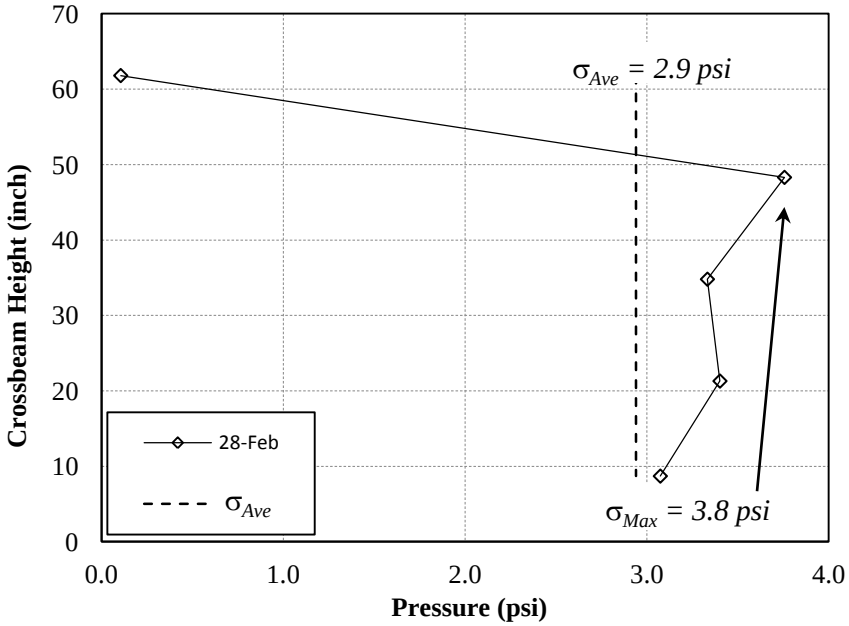

Figure 53 Comparison of actual pressure across SSS height to average (uniform) pressure, column four, February 28th, 2015

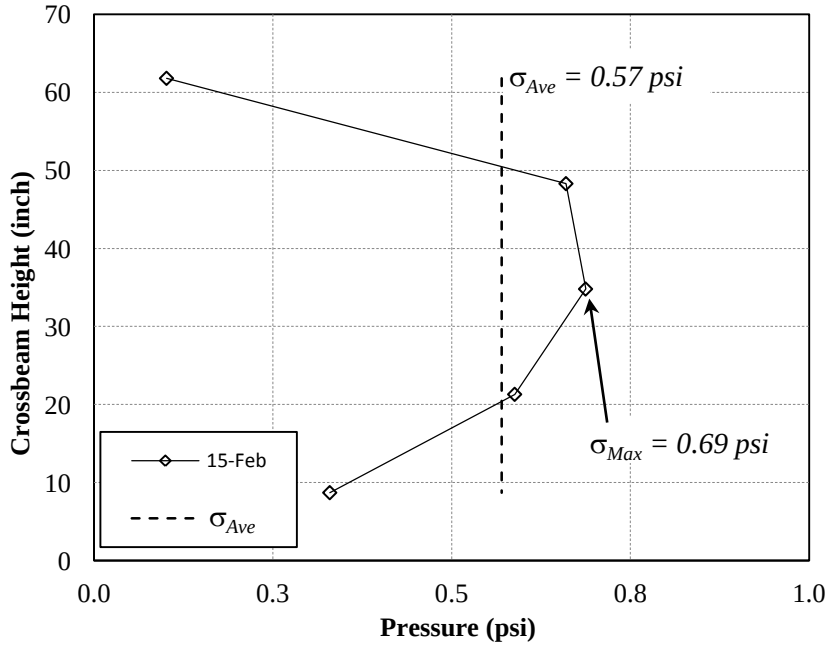

Figure 54 Comparison of actual pressure across SSS height to average (uniform) Pressure, column one, February 15th, 2016

Table 11 Ratio of Maximum-to-Average Snow Pressure by Column Acting on SSS for Winter 2015

Date	Column 1	Column 2	Column 3	Column 4
1/15	1.28	1.29	1.80	2.26
2/1	1.28	1.42	1.71	1.79
2/15	1.82	1.60	1.85	1.75
3/1	3.70	2.08	2.23	1.28
3/15	3.40	2.52	1.78	1.58

Table 12 Ratio of Maximum-to-Average Snow Pressure by Column Acting on SSS for Winter 2016

Date	Column 1	Column 2	Column 3	Column 4
1/15	1.60	1.47	1.72	1.68
2/1	1.45	1.59	1.77	1.54
2/15	1.21	1.28	1.80	1.58
3/1	1.63	2.09	1.28	2.04
3/15	1.82	1.72	1.46	2.33

CHAPTER 5: COMPARISON OF EXPERIMENTAL AND THEORETICAL

5.1 Comparison of Average Snow Pressure

Average (uniform) experimental snow pressures calculated for both seasons are compared to the theoretical slope-parallel snow pressures determined by the Swiss Guide and by McClung's analytical expressions. As presented previously, both expressions for snow pressure depend on depth-averaged snow density, ρ, and snow height, H_o (snow depth sensor data is measured as H_o). McClung's analytical expression also contains explicitly the viscous analog to Poisson's Ratio, ν, which is correlated with snow density, and the glide motion influence factor of D/H_o. The Swiss Guide contains the creep factor, K, which includes the influence of the snowpack Poisson's Ratio (although not given explicitly as a function of ν) and the glide factor, N. The Swiss Guide does not provide any information relating creep factor, K, to Poisson's Ratio, ν, but McClung (1993) states that the Swiss Guide creep factor values shown in Table 1 are based on Equation (18), shown below. McClung (1983) has reported values for Poisson's Ratio of $0.16 \leq \nu \leq 0.38$ for snow densities between 350 and 550 kg/m^3 (21.9 and 34.3 lb/ft^3) and for comparison purposes the limits of $0.15 \leq \nu \leq 0.40$ are used herein. With the upper limit of $\nu = 0.40$ inserted into equation (18), and with slope angle set to $\psi = 37°$, the resulting creep factor is $K = 1.11$. This value is outside the limits of data given in table 1, and would correspond to a basic snow density of greater than $\rho = 0.60$. This snow density as used in the Swiss Guide expression for snow pressure, would represent a very extreme value of depth-averaged snow density.

(18)

Values of average pressure previously provided in tables 9 and 10 are plotted as a function of a quantity called the "body force", $B = \rho g H_o$. The snow density used for each experimental data point is based on the Granite Creek SNOTEL Site #497 recorded density for the given date but increased by a factor of 1.27 as described previously. The snow height used is the perpendicular to ground height, H_o, average recorded value from the three snow sensors.

Two different comparisons for each theoretical model (Swiss Guide and McClung) are provided: one assuming no glide motion whatsoever, and a second with the glide factor equal to that assumed in the design of the Milepost 151 SSS. For the experimental data, no information on glide motion was obtained and thus one must infer the potential for glide motion based on ambient and snowpack temperatures. With reference to figure 41 which shows snowpack temperature nine inch (0.229 m) above the ground (from PC located in row one) during winter 2015, it can be seen that snowpack temperature remained below freezing for data through February 1st. This is a strong indicator that glide motion did not contribute to snow pressure since the snow cover would be frozen to the ground. For experimental data after February 1st, 2015 (i.e. February 15th and on) snow temperatures near the ground were routinely well-above freezing and thus it is likely that glide motion contributed to recorded snow pressures. With these assumptions, experimental data for winter 2015 was separated into a "no glide motion" data group for dates up to and including February 1st, and a "glide motion" data group for experimental points after February 1st. For winter 2016 experimental data, the maximum snow cover temperatures near the ground were below freezing for all data through March 1st, and this information is included in the "no glide motion" data set. Data points for the March 15th, 2016

date are assigned to the "glide motion" data set based on snow cover temperatures well-above freezing near the ground for this two-week period. For the theoretical snow pressures, the analytical expressions given previously are used with either a) *N=1* (Swiss Guide) or $D/H_o = 0$ (McClung) for the "no glide motion" comparison, or b) $N = 3$ (Swiss Guide) or $D/H_o = 2.66$ (McClung by Equation 11) for comparison with the "glide motion" experimental data group. Also, the theoretical snow pressures given do not include an end-effect factor.

5.1.1 Average Experimental Versus Swiss Guide Snow Pressures

Experimental and the theoretical average snow pressures for "no glide motion" are compared in figure 55 for both winters 2015 and 2016 and for the limits of Poisson's Ratio given previously. Generally, the data is grouped along the lower limit Swiss Guide theoretical line corresponding to $\nu = 0.15$, with 7 of the 24 total data points located above the upper limit Swiss Guide pressures for $\nu = 0.40$. Of the seven data points above the upper Swiss Guide theoretical snow pressure line, two are from column four which experiences end-effects and thus are expected to be much higher than the theoretical values calculated without end-effects included. For the other five data points sitting above the upper Swiss Guide limit, there is no obvious explanation for the difference between experimental and theoretical average snow pressures other than the inherent statistical variability of snow properties and thus pressures. Aside from the five data points above the upper limit (the other two outside the limits are end-effect pressures), it appears the Swiss Guide provides a reasonably accurate estimate of snow pressure in the line of slope for no-glide conditions.

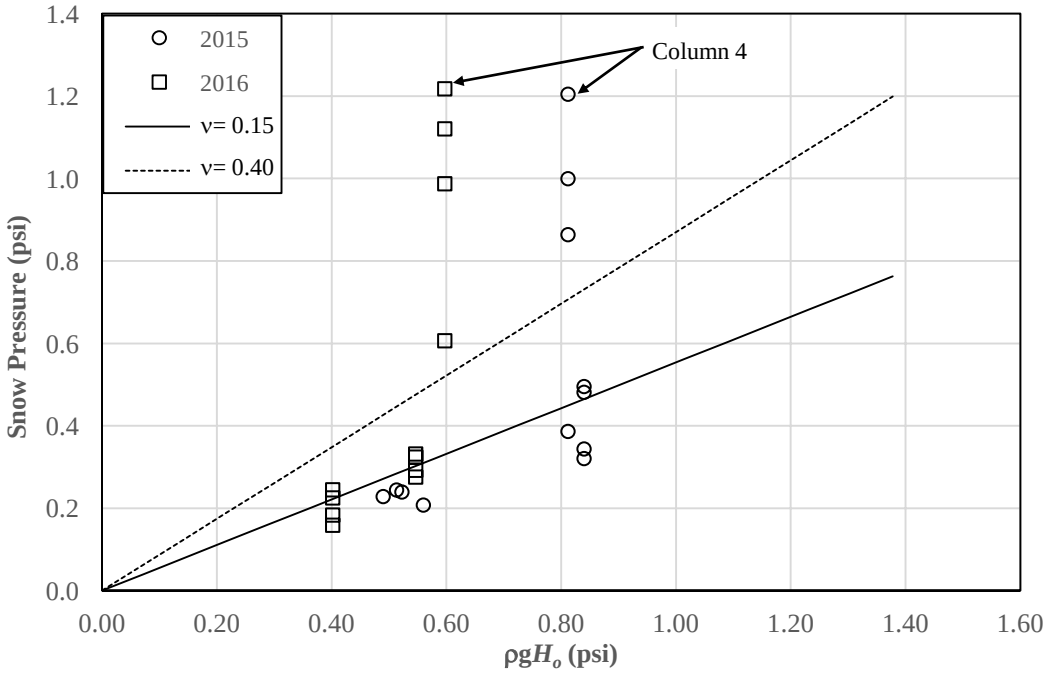

Figure 55 Comparison of experimental and Swiss Guide for average snow pressure without glide (D/H=0), n=24

Figure 56 presents the experimental versus theoretical average slope-parallel snow pressures for the glide motion condition. Of the 20 data points in this data group, all but 3 are located below the upper Swiss Guide snow pressure line, and 2 of the 3 are pressures at the end-effect region. The experimental data for glide motion are not as linear as the no-glide data set seen in figure 55.

Overall, it appears that the upper Swiss Guide snow pressure limit provides a reasonable upper bounds to snow pressures when glide conditions are present.

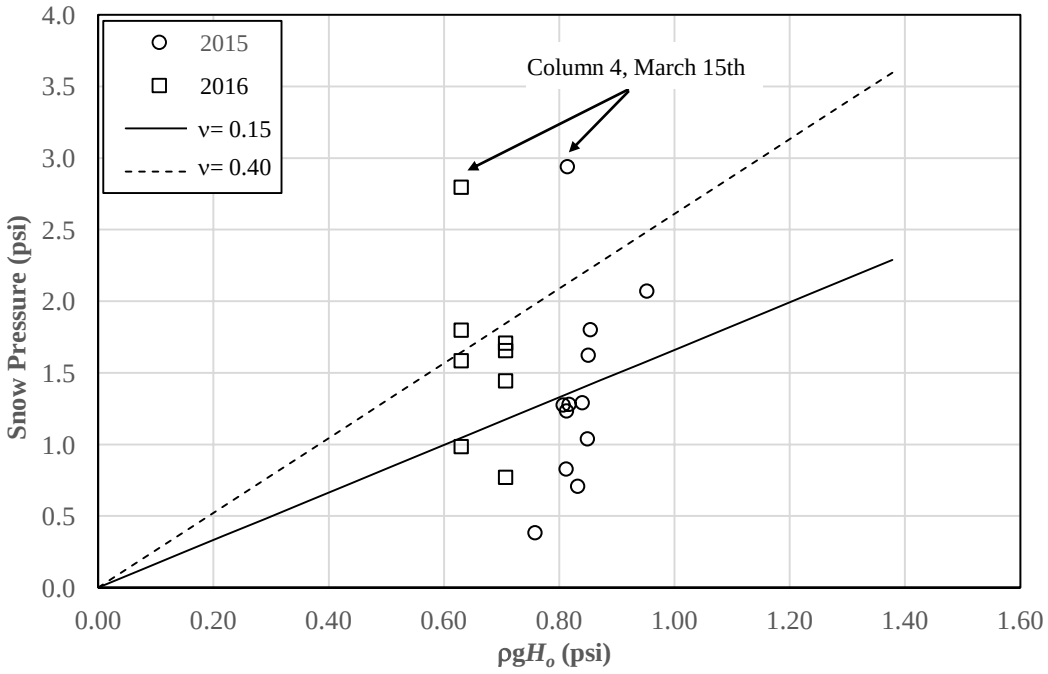

Figure 56 Comparison of experimental and Swiss Guide for average snow pressure with glide (D/H=2.66), n=20

5.1.2 Average Experimental Versus McClung Model Snow Pressures

Experimental and the theoretical average snow pressures for "no glide motion" are compared in figure 57 for both winters 2015 and 2016 and for the limits of Poisson's Ratio given previously. It can be seen that much of the data is grouped along the theoretical line corresponding to the lower limit of Poisson's Ratio, with 7 of the 24 total data points located above the upper theoretical snow pressure limit based on $\nu = 0.40$. Of the seven points above the upper McClung line, two correspond to PC column four, which as shown previously in this report, does indeed experience higher pressures due to end-effects. In whole, McClung's model with a Poisson's Ratio of $\nu = 0.15$ appears to provide an accurate estimate of snow pressures when glide motion attributed component is not present.

A comparison of experimental and theoretical average snow pressures for the "glide motion" case is provided in figure 58. Of the twenty experimental data points, six are located above the upper limit for snow pressure corresponding to $\nu = 0.40$. Twelve of the data points are located below the lower limit snow pressure line corresponding to on $\nu = 0.15$. Two of the highest snow pressure experimental values correspond to PC column four for the March 15th date. It is likely that end-effects coupled with high glide rates of late spring under very warm conditions contributed to these extreme values. It is stressed that the McClung expression snow pressures do not account for end-effect pressures and thus it is not unexpected that average pressures from the free edge of the SSS during late spring are much greater than the snow pressures given by McClung's equations including glide effects. Taken as a whole, McClung's analytical expression with the upper limit of on $\nu = 0.40$ appears to give a good upper limit estimate for average snow pressure. It is also critical to note that the theoretical values presented for the "glide motion" case

assume the above given values of glide factor, *N*, (Swiss Guide) and stagnation depth, D/H_o (McClung). Experimental determination of the exact factors for glide motion is complex and requires continuous access to the site so that actual deformations within the snow cover can be measured. With no such data, a complete understanding of the experimental data obtained is difficult since two phenomena influence the "glide motion" snow pressures: surface roughness conditions and end-effects.

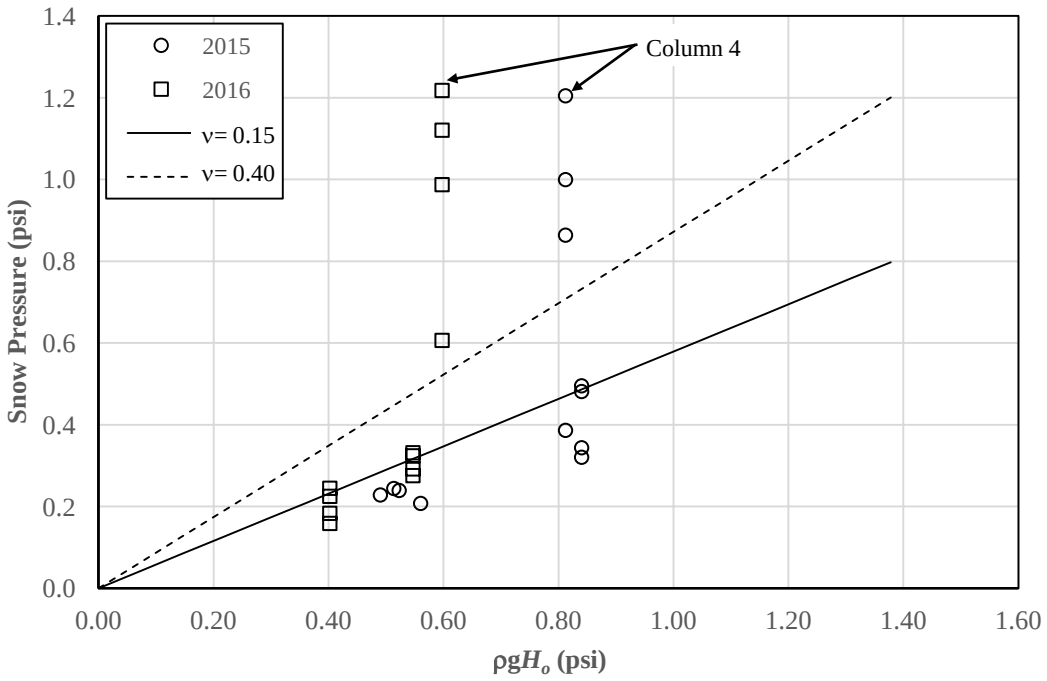

Figure 57 Comparison of experimental and McClung for average snow pressure without glide (D/H=0), n=24

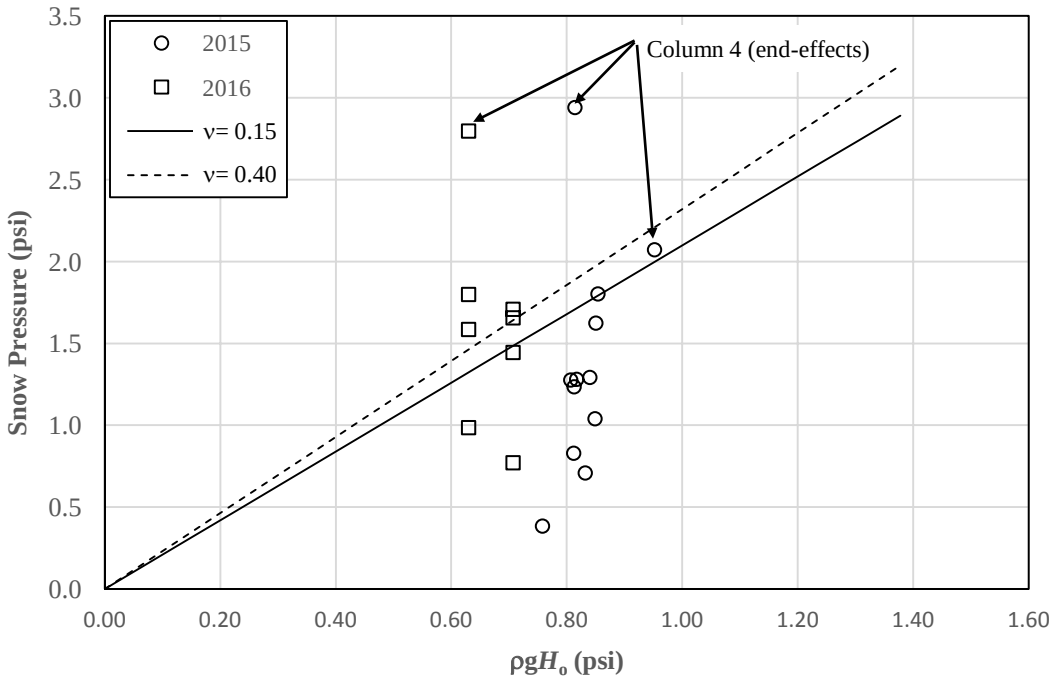

Figure 58 Comparison of experimental and McClung for average snow pressure with glide (D/H=2.66), n=20

5.2 Comparison of Maximum Average Experimental and Swiss Guide Pressures

The snow pressures used in the design of the Milepost 151 SSS were based on an assumed maximum vertical snow height of 78 inch (1.98 m), average slope angle of $\psi = 35°$, and glide factor of $N = 3$. The only other parameters needed in the Swiss Guide equation for slope-parallel snow pressure is the snow density, ρ, and creep factor, K. The elevation of the Milepost 151 site was taken as 7200 ft (2194.6 m) during design of the facility, which yielded an altitude factor of $f_c = 1.14$ and a basic snow density of $\rho = 1.14 \times 0.27 = 0.308$. It is important to state that this snow density determined by the Swiss Guide is not the final assumed maximum depth-averaged snow density that would occur after settling of the snow cover in late springtime. To account for this density increase with vertical snow settlement, the Swiss Guide applies one additional, indirect increase to the snow pressure formula: the snow pressure given by equation (2) is increased by a factor of 1/0.77 = 1.30. This implies a snow density of 1.3 x 0.308 = 0.400 for the Milepost 151 site. The creep factor calculated originally in design, based on data in table 1 (from Swiss Guide) and interpolated for the snow density of $\rho = 0.308$ and for the above slope angle was $K = 0.72$.

Actual values of the above key parameters should be used when comparing experimental to theoretical snow pressures. The measured slope angle at the instrumented SSS was $\psi = 37°$. For interior column snow pressures (i.e. no end-effects), the maximum average snow pressure occurred between March 1st and 15th, 2016, and was $\sigma_{Ave} = 1.8$ psi (12.4 kPa) (see table 10, column three pressure). The snow density concurrent with this pressure value, as extrapolated from the Granite Creek SNOTEL site was $\rho = 0.390$ (1.3 *x* 0.30 = 0.390; see figure 19 for snow density). The *vertical* snow cover height when the maximum seasonal average pressures were experienced was $H = 60$ inch (1.524 m). The snow creep factor corresponding to the above actual density on March 15th is taken from table 1 as $K = 0.83\ x\ \sin(2x37°) = 0.798$. With all of these

values set to the measured data, and using the Swiss Guide snow pressure formula equation (2), the slope-parallel average snow pressure without end-effects is:

(8.96 kPa)

This pressure is not increased by the factor of 1/0.77 = 1.3 described above because the actual snow density concurrent with the maximum average pressure was used. Thus, the actual maximum uniform (average) snow pressure experienced away from the end-effect region was approximately 38 percent greater than that predicted by the Swiss Guide (1.8/1.3 = 1.385 or 38.5 percent).

For maximum uniform snow pressure within the end-effect region, an average pressure of σ_{Ave} = 2.9 psi (20.0 kPa) was calculated for the March 1st, 2015 data set (see table 9, column four pressure). The corresponding snow density was $\rho = 0.40$ (1.3 *x* 0.308) and the *vertical* snow height was $H = 70$ inch (1.778 m). The snow creep factor corresponding to the above actual density on March 1st is taken from Table 1 as $K = 0.83\ x\ \sin(2x37°) = 0.798$. With an end-effect factor calculated per the Swiss Guide formula (see *Section 2.2.2*) of $f_R = 4.75$, and other variables set to the measured data, the slope-parallel average snow pressure with end-effects is:

(60.0 kPa)

Thus, the actual maximum uniform pressure in the end-effect region was 33 percent of that predicted by the Swiss Guide (2.9/8.7 = 0.33 or 33 percent).

5.3 Comparison of Maximum Average Experimental and McClung Pressures

If the same values provided above for the Swiss Guide comparison are used in the McClung Model, average design snow pressures of the McClung Model can be calculated. From equation (18), a Poisson's Ratio corresponding to the creep factor determined from the Swiss Guide of $K = 0.798$ is found by solution for ν:

Using this value, the factor for SSS boundary condition from equation (11) is:

By equation (12), the dimensionless glide ratio is determined by setting the glide factor, $N = 3$ and solving for, D/H_o:

McClung's average snow pressure expression given as equation (13) previously, uses snow height normal to the ground surface, H_o. Heights corresponding to the dates used above are H_o = 60 inch x *cosine* (37°) = 47.9 inch (1.217 m) for the March 15th, 2016 date, and H_o = 70 inch x

cosine (37°) = 55.9 inch (1.420 m) for the March 1st, 2015 date. The average design snow pressure outside of the end-effect region by McClung's analytical model is:

(10.2 kPa)

Therefore, the ratio of experimental maximum uniform snow pressure to that predicted by McClung's Model for no end-effects is 1.8/1.48 = 1.22; experimental average pressure away from end-effect zone was 22 percent greater than that predicted by the McClung analytical expression. For the predicted average snow pressure at the end-effect zone, the Swiss Guide end-effect factor must be used since the McClung equations do not include end-effects:

(68.8 kPa)

Therefore, the ratio of experimental maximum uniform snow pressure to that predicted by McClung's Model when end-effects according to the Swiss Guide are used is 2.9/9.98 = 0.29; the experimental average pressure in the end-effect zone was only 29 percent of that predicted by the McClung analytical expression.

5.4 Comparison of End-Effect Factor

For SSS that are very wide (along a contour), average snow pressures near the interior and away from the free edges can be taken as those given in either the Swiss Guide or by McClung's Model without end-effects. Where end-effects are likely to be present, the end-effect factor, f_R, is used to increase the basic average interior pressures. The season-averaged end-effect factors presented previously were f_R = 3.5 and 0.7 for winter seasons 2015 and 2016, respectively. These corresponded to dates when glide motions were deemed to be present. The maximum observed end-effect factor was f_R = 4.9 which occurred during the last bi-weekly period in March of 2015. The Swiss Guide end-effect factor for the original design of the Milepost 151 SSS was f_R = 4.75. The ratio of maximum experimental end-effect factor to that given by the Swiss Guide is 4.9/4.75 = 1.03, and thus the experimental data correlates extremely well with the Swiss Guide factor. Based on this, it can be said that the Swiss Guide provides a reasonable estimate on the influence of the end-effect phenomenon. It is not readily apparent why the end-effects were so much less significant for the winter 2016 snow pressures, as compared to the 2015 data.

CHAPTER 6: PERFORMANCE AND CONDITION OF SSS

6.1 Performance Evaluation

Evaluation of the performance of the Milepost 151 facility included visual observations of the site from the valley floor by WYDOT avalanche technicians during winter periods. For performance assessment, the primary metric being monitored was frequency of avalanching at the site, including any avalanches onto the roadway below or smaller slides that are contained within the facility. The Milepost 151 facility has been in place and operational since the winter season 2012 – 2013. During this five years of service, no avalanches large enough to reach the roadway have occurred and the project has allowed WYDOT winter maintenance to manage other local avalanche hazards without any attention to the Milepost 151 site.

Despite the overall success of the 151 facility, there have been small avalanches that have released but that were contained within the series of 87 SSS. Specifically, on January 18th, 2015, a small release in the upper reaches of the starting zone occurred and impacted several SSS below the release zone. Figure 60 below shows a zoomed-in photograph of the slide area taken from the valley floor. The small avalanche released from just above and to the (viewer's) left of the instrumented SSS and impacted it and the SSS row immediately below it. In order to assess whether any damage to SSS or to the instrumentation was present, special permission to access the site was granted by the USFS and InterAlpine personnel hiked up to the slide area. Figure 61 shows a photograph of the avalanche debris resting on the lower SSS row as viewed from the instrumented SSS. While debris was observed to be "caught" by the top of the instrumented SSS, no damage to the instrumentation was observed.

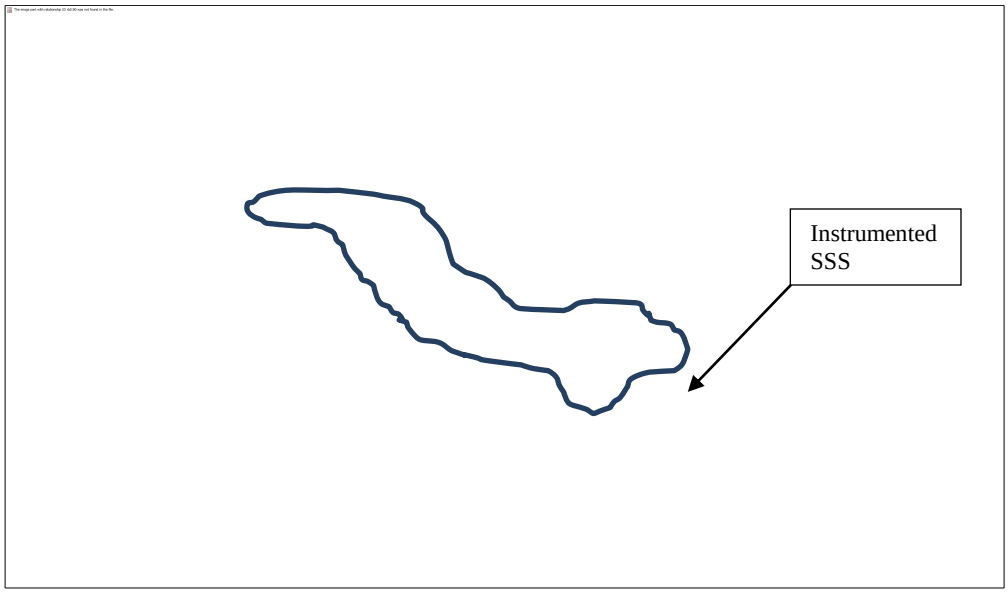

Figure 59 Extents of small avalanche in upper reaches of the Milepost 151 site, January 2015.

Figure 60 Avalanche debris resting on SSS at the Milepost 151 Avalanche site.

6.2 Visual Inspection of SSS Facility

6.2.1 SSS Condition Assessment

Visual inspection of the Milepost 151 facility was conducted during the summertime of 2014, 2015, 2016, and 2017 to identify the overall condition of the SSS. Specific items focused on during the site visits included micropile foundations and connections to the SSS, individual members including crossbeams, struts, and girders, and connections between members including bolted and welded connections.

After five years of service the Milepost 151 facility is overall in excellent condition. The weathering steel components of the SSS have developed a robust surface layer of rust, or patina, which serves to protect the remainder of steel underneath the layer. This is visible in figure 62 which shows the row of SSS at the location of the instrumented SSS. There does not appear to be any locations within the structural steel of the SSS units that collect and retain moisture, and this is critical since prevention of additional steel corrosion requires cycles of wetting and drying and no standing water on steel.

Inspection of the above-ground portion of micropile foundations and their connections to the SSS have revealed some issues that may require maintenance in the future. Almost all of the visible hollow-core micropile bar protruding from the ground has the factory applied epoxy paint intact and in excellent shape. However, there are SSS across the entire site with micropile bar couplers with either partially chipped epoxy paint or without paint altogether. An example of this is displayed in figure 63, which is SSS #3 (numbering per the original construction documents and shown in figure 6). Other couplers have some epoxy remaining as shown in figure 64. There are SSS that have couplers with fully intact epoxy coating, and these were typically observed to be couplers that had the epoxy applied by the manufacturer versus the field-applied epoxy on couplers that required extensions during the original construction of the project. Other non-weathering steel parts of the SSS are also exhibiting some corrosion and this includes the micropile nuts and washers at the lower (strut) foundations, as shown in figure 65.

Although a corrosion rate analysis would likely indicate that parts lacking paint completely will still function safely for up to fifty years, it would be prudent and relatively easy to clean and re-apply an epoxy paint to non-weathering steel components experiencing the most significant corrosion. It is estimated that a two-man crew could complete this task in about a one week time frame, at an estimated cost on the order of a few thousand dollars. It may be that this work is required periodically, say every five to seven years, over the life of the facility.

Inspection of SSS struts, girders, and crossbeams has not revealed any visible signs of distress to date. For example, if the SSS was overloaded, one likely noticeable feature would be permanently deformed crossbeams and this has not been observed. Inspection of welded and bolted connections also indicates overall excellent performance of the facility, but with one exception. Structure #16 has a strut-to-girder connection with a nut almost completely off of the bolt as shown in figure 66. It is likely that this condition has been present since the end of construction but should be verified in the field by maintenance personnel. The side plate connection of strut to girder was also of particular interest during the inspections as this appears to be a slender structural element. Figure 67 shows a severely bent side plate on SSS #1. However, it is believed that this was caused by overtightening of the connecting bolt at the connection and not due to structural over-loading of the SSS.

The final aspect noticed during each summer assessment is misalignment of struts with their micropile foundations. Ideally, during construction the micropile foundation bars would be installed in a plumb orientation when viewed from downhill and looking towards the SSS. In other words, micropile bars should not "lean" to the left or to the right, and these should be aligned with the also plumb strut. Although some misalignment possibly occurred during the original construction project, there is the possibility that lateral or across-slope SSS loading could induce enough bending in micropile bars to cause a misalignment of strut and foundation axes. The extent to which this has occurred is not known, but structures 41,56, 73, 80 have struts and foundations with noticeable misalignment, and shown in figure 67. It is advisable to periodically inspect these specific structures to monitor whether the misalignment is worsening or has stabilized.

6.2.2 Condition of Reforestation Aspect of Facility

A significant aspect of the original construction project was provision for reforestation across the site with native conifer species. This was a result of part of the NEPA approval process during the project development, and aimed to mitigate the visual impacts of the project to the surroundings. The intent of the reforestation was not to add to the starting zone stabilization effects of the SSS, but simply to provide screening to some portions of the site so that the SSS are less visible. Although initially the loss rate of replanted trees in the first two years was over 50 percent, this aspect of the project has been partially successful with many of the whips now firmly established and with height on the order of four feet or more, as shown in figure 66. However, future loss of some of these surviving trees is likely due to failing landscape benches that provided the necessary soil bedding during original planting in 2012 and 2013. This is exhibited in figure 67 which shows healthy conifers immediately above a mostly failed soil bench.

Figure 61 Row of SSS at upper region of starting zone; SSS chosen for instrumentation is at left side of photo

Figure 62 Example of corrosion on micropile foundation coupler without epoxy paint

Figure 63 Example of epoxy paint missing on foundation connection couplers

Figure 64 Chipped epoxy paint on strut foundation nut and washers

Figure 65 Strut connection with nut almost off of bolt

Figure 66 Deformation of strut-to-girder connecting plate due to over-tightening of bolt on SSS #1

Figure 67 Misalignment of strut axis and micropile axis on structure #73

Figure 68 Successful re-growth of evergreens below SSS

Figure 69 Re-growth of evergreens with failed landscape bench

CHAPTER 7: SUMMARY, CONCLUSIONS, AND RECOMMENDATIONS

7.1 Summary

This research report has documented the results of an experimental program where snow pressures acting on a rigid SSS in an avalanche starting zone were monitored over two winter seasons. Snow pressures were recorded using pressure transducers mounted across the height and width of the grate surface of the SSS to obtain pressure versus height and depth profiles and also capture snow pressure time-dependence. The experimentally measured snow pressure data was manipulated to calculate various snow pressure parameters that are typically used by the design professional including average (uniform) snow pressure, total snow resultant force and its location along the SSS height, the ratio of maximum snow pressure to average snow pressure, and the increase of snow pressures at the end-effect region of a SSS. Key aspects of the experimental data were then compared to values predicted by the most commonly used design guide for snow supporting structures placed in an avalanche starting zone, the "Swiss Guide". The results of this research work provide the needed verification of the applicability of the Swiss Guide provisions where an irregular pattern of SSS is used to cover an avalanche starting zone, and will inform design engineers in the United States on how the European design standard is applied for projects within the Unites States.

7.2 Conclusions and Recommendations

Based on the experimental and analytical work documented in previous chapters of this report, the following qualitative statements can be made. Snow pressure temporal and spatial variation over a winter season followed the expected basic patterns, including:

- Increasing snow pressure with height of snow cover.
- Non-uniform parabolic pressure with depth profile, increasing to a maximum near mid-height of snowpack and decreasing closer to ground surface.
- Increasing pressure as snowpack densifies as the winter season progresses.
- Increasing snow pressure as degree of proximity to free edge increases, where free edge has no adjacent SSS.
- Increasing snow pressure with springtime warming of snowpack during the daylight hours, i.e. glide effects.
- Diurnal variation of snow pressure where maximums occurs in late afternoon with daytime high temperatures and then reduction in pressure upon freezing at night and re-freezing to ground surface.

7.2.1 Average Slope-Parallel Pressure for Design

The maximum observed average pressure across the two winter seasons was 1.80 psi (12.4 kPa) in the interior of the SSS and away from the end-effect zone. This is 38 percent and 22 percent greater than the values determined using the theoretical models of the Swiss Guide and McClung, respectively. With a 1.6 snow load factor used in the strength design of the SSS, it appears that either model can be used to provide the uniform snow pressure to be applied across the full height of a SSS and over a width not including the end-effect region.

Within the end-effect region, the maximum average pressure observed was 2.9 psi (20.0 kPa) while the Swiss Guide and McClung models predicted pressures of 8.7 psi (60.0 kPa) and 10 psi (68.9 kPa), respectively. Therefore, both models appear to be excessively conservative for end-effect pressures. However, the width over which the increased end-effect loading is applied is relatively small: for the Milepost 151 site the end-effect length per the Swiss Guide was ΔL = 1.80 ft (0.549 m). This distance only amounts to 15 percent of the 12 ft (3.658 m) wide SSS unit used at the Milepost 151 site. It is felt that the seemingly excessive conservatism of the Swiss Guide for end-effect pressures will not dramatically change the design of a SSS, and it is recommended that the Swiss Guide is used as-is until additional information can be obtained to justify lowering these pressures.

7.2.2 Location of Snow Force Resultant on SSS

During the course of design of a SSS, overall global equilibrium of the SSS depends on the total snow force resultant, R_N, and the location where it is assumed that it acts along the height of the SSS. The magnitude of total snow force resultant predicted by the Swiss Guide was shown to be reasonably close to the experimental values by comparison of average snow pressures, albeit slightly higher as noted above. The location of resultant in the Swiss Guide is assumed to act at mid-height of the SSS and foundation reactions forces are determined with this assumption. The experimental data indicates a resultant location slightly higher than mid-height – 0.56 times the height of the SSS. It is recommended that this height be assumed for overall equilibrium calculations in the design of rigid SSS.

7.2.3 Ratio of Maximum-to-Average Snow Pressure

For local member design, the Swiss Guide stipulates an increase in the basic snow pressure determined by equation (2) and (3) to account for late-season densification of snowpack and thus higher snow pressures. This is accomplished by dividing the basic uniform pressure by 0.77 which implies an increase of 30 percent when designing say crossbeams, or girders, or struts. This pressure is not applied over the full height of the SSS for use in determining foundation reactions – it is used only for "local" member design. In section 4.8 of this report, it was shown that maximum localized pressures (near mid-height) are on average 1.8 times greater than the uniform pressure applied to the full height of SSS. Based on this, it is recommended that local member design (away from the end-effect region) be based on the average (uniform) pressures by either the Swiss Guide or McClung but increased by a factor of 1.8. It is not recommended to increase end-effect pressures by this amount due to the apparent excessive conservatism of end-effect pressures by the two models.

7.2.4 Design by Swiss Guide for Irregular SSS Deployment Configurations

One of the important aspects of this project included the validation of the Swiss Guide as a design standard when a highly irregular pattern of SSS is used across the starting zone. The long, linear rows of SSS used in Europe create uniform pressure profiles in the back-pressure zone upslope of the SSS and in between rows of SSS. This is not the case at the Milepost 151 site where the more distributed layout pattern of SSS requires complex load paths within the snowpack to be developed in order for the SSS array to support it adequately. From a reduction of large avalanches perspective, the irregular pattern appears to be an acceptable alternative to more regular SSS layouts. From a snow pressure point of view, the measured pressures were only slightly greater than those given by theory and the differences could be attributed to the irregular SSS plan. However, the pressure differences were not so large that a modification to

theoretical pressures to account for plan irregularity is warranted. Moreover, this experimental study provides data on behavior for one specific layout of SSS, and it is not possible to develop design guidelines for irregular layout patterns based solely on this particular study. But it should be stated again that there appears to be reasonable agreement between experimental and Swiss Guide pressures, and the Swiss Guide should continue to be used by design professionals practicing within the United States.

Finally on the irregular, staggered layout of SSS to minimize visual impact, it appears that if the Swiss Guide provisions for maximum slope distance between SSS are followed, the irregular pattern can be adopted. More extensive details on the Milepost 151 irregular layout design can be found in the project engineering design report by InterAlpine Associates, LLC. However, the basic principle is that no "tile" of snowpack uphill from a SSS and within the starting zone has a length greater than the maximum distance between SSS per the Swiss Guide, and that all areas within the starting zone are covered by the SSS "tiles". A tile is the width of the given SSS (or grouping of SSS) and the uphill (along-the-slope) distance to the next SSS.

7.2.5 Site-Specific Layout Design Versus Unit Design

The original design approach for the Milepost 151 project was influenced by the lack of any precedent in the United States for use of rigid steel structures in an avalanche starting zone for avalanche mitigation, and the desire to produce a problem-free facility that functions as intended. Because of the irregular layout scheme, single units were expected to potentially experience very high total snow loads because of the presence of end effects at both sides of the SSS. SSS units arranged in doubles and triple arrangements on the other hand would theoretically experience proportionately less intense snow loads for much of their interior. However, for the simplicity of construction, a "unit design" approach where a single design of an isolated SSS with end effects at each side was adopted. This single design was applied to all SSS at the site irrespective of whether it was stand-alone or located in a double or triple grouping. For future projects, based on the success of the operating Milepost 151 facility and based on the findings of this particular research project, it is recommended that different designs of SSS be made for single units, double units, triple units, etc. The consequence of this approach will be slightly reduced material costs for structural steel (units used in groups will be able to use smaller members) and potentially in labor if foundations are also designed specific to the given SSS arrangement (i.e. single unit, double, etc). The additional engineering expense to make multiple designs of SSS based on their location within a site layout is not expected to outweigh the above cost savings.

REFERENCES

De Biagi, V., barber, M., Barpi, F., Brunetto, M., Bovet, E., Chiaia, B., Pallara,O., Maggioni, M., Ceaglio, E., Freppaz, M., Viglietti, D., Zanini, E., and Segor, V., 2013. An Integrated System to Assess Snow Forces on Avalanche Defense Structures from Snow Gliding: La Tour Test Site – Aosta Valley (IT). In the Proceedings of the International Snow Science Workshop Grenoble – Chamonix Mont-Blanc, 2013, pp. 1340-1345.

Federal Office of the Environment (FOEN), 2006. Defense Structures in Avalanche Starting Zones, Technical Guidelines as an Aid to Enforcement. WSL Swiss Federal Institute for Snow and Avalanche Research, Davos, Switzerland.

Haefeli, R., 1948. Schnee, Lawinen, Firn, und Gletscher. Enginieur – Geologie, pp. 663-735.

Larsen, J., McClung, D., and Hansen, S., 1985. The Temporal and Spatial Variation of Snow Pressure on Structures. Canadian Geotechnical Journal, Vol 22, pp. 166-171.

McClung, D., 1982. A One-Dimensional Analytical Model for Snow Creep Pressures on Rigid Structures. Canadian Geotechnical Journal, Vol 19, pp. 401-412.

McClung, D., Larsen, J., and Hansen, S., 1984. Comparison of Snow Pressure Measurements and Theoretical Predictions. Canadian Geotechnical Journal, Vol 21, pp. 250-258.

McClung, D., and Larsen, J., 1989. Snow Creep Pressures: Effects of Structure Boundary Conditions and Snowpack properties Compared with Field Data. Cold Regions Science and Technology, Vol 17, pp. 33-47.

McClung, D.,1993. Comparison of Analytical Snow Pressure Models. Canadian Geotechnical Journal, Vol 30, pp. 947-952.

ACKNOWLEDGEMENTS

The authors would like to thank the Wyoming Department of Transportation (WYDOT) and the Federal Highways Administration (FHWA) for funding this project. Additionally, a special thanks to Jamie Yount and John Eddins (both formerly of WYDOT), Rand Decker, Sean Strain, and graduate student Megan Stevens. Finally, thank you to Tim McDowell and Enid White of the WYDOT Research Center and to the members of the WYDOT Research Council.